Eigenstate assignments and the quantum-classical correspondence for highly-excited vibrational states of the Baggot H_2O Hamiltonian

Srihari Keshavamurthy[a] and Gregory S. Ezra
Baker Laboratory, Department of Chemistry, Cornell University, Ithaca, New York 14853

(Received 24 September 1996; accepted 28 March 1997)

In this paper we study the classical and quantum mechanics of the 3-mode Baggot vibrational Hamiltonian for H_2O. Our aim is to classify and assign highly-excited quantum states based upon a knowledge of the classical phase space structure. In particular, we employ a classical template formed by the primary resonance channels in action space, as determined by Chirikov resonance analysis. More detailed analysis determining the exact periodic orbits and their bifurcations and families of resonant 2-tori for the Baggot Hamiltonian confirms the essential correctness of the Chirikov picture. It is emphasized that the primary periodic orbits alone do not define a suitable phase space skeleton; it is important to consider higher dimensional invariant structures, such as 2-tori and 3-tori. Examining the manifold of quantum states for a given superpolyad number $\mathsf{P}=n_1+n_2+n_b/2$ reveals sequences of eigenstates that progress along the classical resonance zones. These sequences provide insight into the nature of strongly mixed states found in the vicinity of the resonance junction. To further explore the classical-quantum correspondence, we have also computed eigenstate Husimi phase space distribution functions and inverse participation ratios. It is thereby possible to provide dynamically based assignments for many states in the manifold of states with superpolyad number $\mathsf{P}=16$. © *1997 American Institute of Physics.*
[S0021-9606(97)01425-6]

I. INTRODUCTION

Understanding the nature of highly-excited vibrational and rotation-vibration states of polyatomic molecules is a problem of central importance in chemical physics.[1] Traditional spectroscopic methods for assignment of levels based on harmonic oscillator (normal mode)-rigid rotor quantum numbers and wavefunctions[2] can break down for highly-excited rovibrational states as a result of strong mode coupling.[3,4] Such mode coupling, due either to anharmonic coupling terms in the potential or to rotation-vibration interaction, leads to the phenomenon of intramolecular vibrational energy redistribution (IVR),[4] and results in complicated energy level and intensity patterns.

One source of apparent complexity in vibrational spectra is strong mixing of manifolds of near-degenerate states by a single resonant coupling term; the corresponding classical problem is nevertheless integrable in this case. Another possibility is strong mixing of states due to the presence of two or more resonant coupling terms; classically, the problem is nonintegrable and we have the possibility of chaos.[5] State mixing can also occur as a result of *dynamical tunneling*,[6] a nonclassical mixing of states localized in different regions in phase space that is associated either with symmetry related or accidental degeneracies of levels.

Many approaches have been proposed for the study of complicated spectra beyond traditional methods: we mention statistical Fourier transform analysis,[7] hierarchical trees;[8] periodic orbits;[9,10] semiclassical propagator based approaches;[11] and bifurcation theory.[12,13] Recently, Wolynes and coworkers have made efforts[14–17] to understand IVR and eigenstate localization in large systems by establishing connections to the problem of Anderson localization in the theory of disordered metals.[18]

Considerable progress has been made in the analysis of two modes coupled by a single resonant term.[12] In this case there is a constant of the motion in addition to the total energy, and the associated reduced phase space is a 2D *sphere*, the so-called polyad phase sphere.[19] Classically, one can study the fixed points of a reduced 1 degree-of-freedom (dof) spectroscopic Hamiltonian on the sphere, which correspond to periodic orbits (pos) in the full phase space. These fundamental periodic orbits serve as organizing centers for the classical and quantum phase space. As parameters such as energy or polyad number are changed, these periodic orbits will bifurcate or merge, leading to qualitative changes in the phase space structure. Each distinct arrangement of periodic orbits and associated stable and unstable manifolds (for unstable pos) defines a *zone* in parameter space, and Kellman and coworkers[20] have systematically studied the bifurcation of pos and the passage from one zone to another for both 1:1 and 2:1 resonant systems (see also the recent work of Joyeux[21]). Periodic orbit bifurcations in 1:1 and 2:1 resonant vibrational Hamiltonians have been studied using semiclassical energy-time analysis[22] of level spectra.[23]

It is of considerable importance to extend such approaches to deal with multi-mode ($N\geqslant 3$) systems. More generally, we seek to develop qualitative methods for analysis of energy level patterns and wavefunctions in multimode systems based on the underlying classical nonlinear dynamics.

One possibility, following the success of the polyad

[a]Present address: Department of Chemistry, IIT Kanpur, U.P. 208016, India.

 0021-9606/97/107(1)/156/24/$10.00

phase sphere approach for 2-mode systems, is to determine fundamental pos for multimode Hamiltonians (cf. Appendix). Lu and Kellman[24] have recently examined fundamental pos and their bifurcations in a classical version of the 3-mode vibrational spectroscopic Hamiltonian for H_2O due to Baggot.[25] The Baggot Hamiltonian[25] has an extra constant of the motion in addition to the energy, the so-called superpolyad number $\mathcal{N}=2(I_1+I_2)+I_b$ (see next section). In the presence of this additional constant of the motion, the Baggot Hamiltonian has essentially 2 degrees of freedom. Following the procedure used for 2-mode resonant problems, Lu and Kellman have determined critical points of the 2-mode reduced Hamiltonian for H_2O; these critical points correspond to the fundamental pos in the full phase space.[24,26] One can then attempt to use the fundamental pos as a framework for organizing the phase space structure and for understanding the localization of quantum eigenstates.

Another possibility, given the existence of a superpolyad number, is to use the methods of *stratified Morse theory*, as developed in a series of papers by Zhilinskii and coworkers.[13] In this approach a qualitative understanding of the families of pos and their possible bifurcations is obtained on rather general grounds using the powerful mathematical apparatus of Morse theory.

In the present paper, we aim at the construction of a ''classical template,'' based on an approximate partition of the classical phase space, that can be used to understand and organize highly-excited quantum eigenstates. The partitioning of classical phase space is achieved using Chrikov resonance analysis.[27]

An important aspect of the study of the phase space structure of multimode systems is the search for ways to partition (either approximately or exactly) phase space (full or reduced, at constant E) into regions corresponding to qualitatively different dynamics. In the case that the Hamiltonian of interest has two degrees of freedom, the stable and unstable manifolds of unstable pos have the appropriate dimensionality (codimension one) to divide the energy shell into disjoint regions, and each zone in parameter space is then associated with a different partitioning of the polyad phase sphere.[20] Such partitions have been used in theories of phase space transport in systems with mixed phase space.[28,29] The relevant pos can be determined either as critical points on the polyad phase sphere for the case of a single resonant coupling, or as fixed points on a Poincaré section. For $N \geqslant 3$ mode systems, however, the stable and unstable manifolds of unstable pos do not have sufficiently high dimension to define a partition of phase space. The natural generalization of an unstable periodic orbit for $N \geqslant 3$ mode systems is a *normally hyperbolic invariant manifold* (NHIM) (Ref. 29), which has codimension two. Thus the stable and unstable manifolds associated with a NHIM have the right dimensionality to partition phase space in a manner analogous to the two mode case. Mapping out the NHIMs in a general multimode system is a difficult task and there are essential differences as compared to the unstable po in two dimensions. Detailed discussions of the dimensionality issues of dividing surfaces in multimode systems and appropriate generalizations of unstable pos can be found in Refs. 29–31.

In multimode nonintegrable systems, an approximate partitioning of phase space can be obtained via Chrikov resonance analysis.[27] A *resonance channel* or resonance zone is a region of phase space of full dimensionality consisting of trajectories that are strongly affected by a coupling term in the Hamiltonian corresponding to a single resonance condition on N zeroth-order frequencies.[32] Resonance channels define regions of phase space characterized by particular dynamical behavior; it is therefore natural to use them as the basis for a partitioning of phase space in multimode systems. The totality of resonance channels forms the Arnold web.[33] Phase points can drift along resonance channels, and ''change direction'' at intersections between channels.[34] In three or more degrees of freedom systems this diffusion of the action variables in phase space leads to long time instability.[35,36]

The location and width of resonance channels in a given system can be determined approximately using the standard analysis due to Chirikov.[27] In their pioneering work, Oxtoby and Rice mapped out resonance zones for 2- and multi-mode model molecular Hamiltonians in order to correlate the onset of resonance overlap with statistical unimolecular decay dynamics.[37] Resonance channels have since been mapped out for a number of molecular Hamiltonians,[38–45] and connections with the corresponding quantum systems examined.[39,42,43,45] Of particular interest in multimode classical systems is the possibility of chaotic motion at the intersection of resonance channels.[40,41,43,46] Atkins and Logan[43] studied a three mode coupled Morse system with small anharmonicities and demonstrated the possibility of chaos via the intersection of lowest order resonances. For the specific set of parameters in their paper, various measures of localization (basis dependent) provided adequate means to distinguish between different types of quantum states. No significant classical phase space transport of the Arnold diffusion type was however observed in their system. Moreover, Atkins and Logan did not attempt to analyse in detail individual quantum states and correlate eigenstate features with invariant structures in phase space.

The above studies have established close connections between classical overlapping resonance zones and the phenomenon of IVR in the corresponding quantum systems. In the present paper, we further explore the correspondence at the level of analyzing individual quantum states based on a classical resonance template. Specifically, we examine the problem of assigning highly-excited eigenstates of the 3-mode Baggot vibrational Hamiltonian for H_2O in the manifold of states with $\mathsf{P}=n_1+n_2+n_b/2=16$. Results of our analysis for $\mathsf{P}=8$ have been presented elsewhere.[47]

Our analysis of the 45 eigenstates with $\mathsf{P}=8$ showed that each state in the manifold could be given a dynamical assignment based upon study of the distribution of amplitude in action space and the quantum mechanical phase space distribution function.[47] The only ambiguity in assignment was associated with a narrowly avoided crossing of two levels of the same symmetry. The relatively straightforward assignment process for $\mathsf{P}=8$ can be readily understood in

terms of the underlying classical mechanics, in that the 1:1 and 2:1 primary resonance channels hardly overlap.[47]

In the present paper we extend the Baggot Hamiltonian beyond the limit of strict applicability to H_2O (in particular, well above the energy at which the molecule can become linear) in order to study the dynamically interesting case with $P=16$. Not only does this manifold contain many states (153), but the primary resonance zones overlap, so that we are able to investigate assignment of states in the vicinity of a resonance junction.[43]

Our approach is based upon a close study of the classical-quantum correspondence, taking as our starting point a Chirikov analysis of the resonance channels.[27] Chirikov's method is an approximate, perturbative approach to the phase space structure of multimode systems, in that the different resonances are analyzed independently. The Chirikov resonance analysis can however be refined by determining the location of families of resonant $(N-1)$-tori (2-tori in the case of the 3-mode Baggot hamiltonian) determined in the single resonance approximation. We find that the results of the elementary Chirikov analysis and the more refined analysis are in close agreement, confirming the essential correctness of the Chirikov picture for the Baggot Hamiltonian. Using the classical resonance structure as a guide, we are able to organize eigenstates into families that form readily recognizable sequences *along* the resonance channels. These sequences of states are found to exhibit a distinct periodicity with respect to the distribution of amplitude in action space; this periodicity has a simple origin in the slope of the classical resonance line. The sequences provide one way of determining the ''parentage'' of mixed states near the resonance junction (see below).

We note that Rose and Kellman have very recently presented a detailed study of eigenstate assignment in the $P=8$ manifold for the Baggot Hamiltonian.[48] There are several points of similarity between the Rose-Kellman approach and the analysis given in the present paper and in Ref. 47. For example, identification of resonance zones in the zeroth-order action space is central to both approaches (compare Figure 4 of Ref. 48 and Figure 1 of Ref. 47); Rose and Kellman locate resonance zones and assign states using eigenvalue correlation diagrams and examination of polyad phase spheres in the single-resonance approximation; we employ Chrikov analysis and examination of action space and Husimi phase space distribution functions[47] (see below).

Both Rose and Kellman[48] and we[47] agree on the straightforward assignability of states for the $P=8$ manifold of the Baggot Hamiltonian. As noted above, the primary resonance channels do not intersect in this case, greatly simplifying the dynamics. In the present paper, we tackle the rather more challenging case of the $P=16$ manifold, in which the primary resonance channels overlap. Eigenvalue correlation diagrams for this case (cf. Figure 20) show many broad avoided level crossings, which render the diabat following employed by Rose and Kellman problematic. Further remarks on the relation between our approach and that of Rose and Kellman are given below.

For the Baggot Hamiltonian, inverse participation ratio (IPR) Ref. 49 studies do not show such a clear separation of eigenstates into various types (nonresonant, resonant, mixed) as observed in Ref. 43 (see section IV). Interestingly, IPR values seem to be sensitive to sharply avoided crossings, although small values of the IPR, which are associated with the mixing of many zeroth-order eigenstates, do not necessarily imply that the relevant eigenstate is delocalized in phase space. The classical-quantum correspondence for eigenstates of the Baggot Hamiltonian is studied in detail via the Husimi phase space distribution function.[50] We have found several examples of eigenstates which are delocalized in action space (and hence have small IPRs) but are quite ''clean'' and localized in phase space. The Husimi functions together with the classical resonance analysis enable us to provide dynamical assignments for most states in the $P=16$ manifold.

It is important to observe that, although the Baggot Hamiltonian studied here is an effectively 2 degree of freedom system due to the conservation of $\mathcal{N}$, the structure of the corresponding reduced phase space nevertheless exhibits some complexities not present in 2-mode systems typically studied. In particular, the form of the contours of $\mathcal{H}_0$ in the constant $\mathcal{N}$ plane can lead to some unusual state mixing effects (discussed more fully below).

This paper is organized as follows: In section II we describe the classical and quantum versions of the Baggot Hamiltonian for H_2O.[25] Section III provides a survey of the classical phase space structure of the classical Baggot Hamiltonian. The locations of resonance zones, families of 2-tori, and periodic orbits are discussed. We also describe a useful Poincaré section that provides a global view of the classical phase space structure. Subtleties associated with the 2-sheeted nature of the surface of section are discussed. In section IV we outline the methods used for analysis of quantum eigenstates: action space projection; inverse participation ratios; and Husimi phase space distributions. In section V we examine the quantum-classical correspondence for eigenstates of Hamiltonians that are special cases of the Baggot Hamiltonian, obtained by turning off one or more resonant coupling terms. Section VI is devoted to analysis of eigenstates of the Baggot Hamiltonian itself, while section VII concludes. Technical details concerning computation of periodic orbits and 2-tori are given in an appendix.

II. BAGGOT HAMILTONIAN FOR H_2O

A. Classical Hamiltonian

The classical version of the spectroscopic vibrational Hamiltonian for H_2O derived by Baggot[25] is a three degree of freedom local-mode/bend Hamiltonian which includes two 2:1 stretch-bend resonant terms $\mathcal{H}_\sigma^{2:1}$, $\sigma=1$ or 2, a 1:1 stretch-stretch resonant term $\mathcal{H}^{1:1}$ and a 2:2 stretch-stretch term $\mathcal{H}^{2:2}$:

$$\mathcal{H}=\mathcal{H}_0+\mathcal{H}^{1:1}+\mathcal{H}^{2:2}+\sum_{\sigma=1,2}\mathcal{H}_\sigma^{2:1}, \tag{2.1}$$

where $\mathcal{H}_0$ is the zeroth order Hamiltonian

$$\mathscr{H}_0=\Omega_s\sum_{\sigma=1,2} I_\sigma+\Omega_b I_b+\alpha_s\sum_{\sigma=1,2} I_\sigma^2+\alpha_b I_b^2$$

$$+\epsilon_{ss}I_1I_2+\epsilon_{sb}I_b\sum_{\sigma=1,2} I_\sigma, \tag{2.2}$$

and the resonant interaction terms are

$$\mathscr{H}^{1:1}=\beta'_{12}(I_1I_2)^{1/2}\cos(\theta_1-\theta_2), \tag{2.3a}$$

$$\mathscr{H}^{2:2}=\beta_{22}I_1I_2\cos[2(\theta_1-\theta_2)], \tag{2.3b}$$

$$\mathscr{H}^{2:1}_\sigma=\beta_{sb}(I_\sigma I_b^2)^{1/2}\cos(\theta_\sigma-2\theta_b). \tag{2.3c}$$

Here, $(\{I_s,\theta_s\},I_b,\theta_b)\equiv(\mathbf{I},\boldsymbol{\theta})$ are canonical action-angle variables for the two local mode stretches and the bend mode, respectively, and $\beta'_{12}\equiv\beta_{12}+\lambda'(I_1+I_2)+\lambda''I_b$.[25]

It is important to note that the resonance vectors (1, −1,0), (1,0,−2) and (0,1,−2) are linearly dependent,[51] so that there is a constant of the motion $\mathscr{N}$ in addition to the energy:

$$\mathscr{N}=2\sum_{\sigma=1,2} I_\sigma+I_b. \tag{2.4}$$

It turns out that the 2:2 stretch-stretch resonance (Darling-Dennison coupling[52]) does not significantly affect the classical phase space structure in the regime of interest for this paper, and it is omitted from the Hamiltonian in the resonance analysis described below. It is however straightforward to include this coupling term if required. All of the exact numerical results presented in this paper, classical and quantum, do include the 2:2 stretch-stretch resonance.

B. Quantum Hamiltonian

The quantum version of the Baggot Hamiltonian is obtained via the standard correspondence between action-angle variables and creation-annihilation operators:

$$\hat{a}^\dagger\leftrightarrow I^{1/2}e^{i\theta},\quad \hat{a}\leftrightarrow I^{1/2}e^{-i\theta}. \tag{2.5}$$

Using the above correspondence and expressing the resultant Hamiltonian in a basis of number states $|n_1n_2n_b\rangle$, we obtain Baggot's Hamiltonian[25] with the following mapping of parameters:

$$(\beta_{12},\beta_{22},\lambda',\lambda'')\leftrightarrow 2(\lambda,\gamma,\lambda',\lambda''),\ \ \beta_{sb}\leftrightarrow\frac{1}{\sqrt{2}}k_{sbb}, \tag{2.6}$$

where λ and k_{sbb} are defined in Ref. 25. Values of the various parameters are taken from Baggot's fit to the vibrational levels of H_2O (Table II of Ref. 25).

The *superpolyad number*, $\mathsf{P}=\Sigma_{\sigma=1,2}n_s+n_b/2$, is a constant of the motion for the quantum Baggot Hamiltonian. A given value of P is associated with a corresponding classical invariant $\mathscr{N}=2\mathsf{P}+5/2$. Our eigenenergies are shifted with respect to those reported in Ref. 25 by the ground state energy

$$E_{\rm gs}=\Omega_s+\frac{1}{2}\Omega_b+\frac{1}{4}(2\alpha_s+\alpha_b+2\epsilon_{sb}+\epsilon_{ss}). \tag{2.7}$$

TABLE I. Comparison of the parameters used in the paper and parametes from Baggot's fit to the spectroscopic Hamiltonian for H_2O.

Baggot[a]	Paper[b]	cm^{-1}
$\tilde{\omega}_s$	Ω_s	3885.57
$\tilde{\omega}_b$	Ω_b	1651.72
x_s	α_s	−81.99
x_b^*	α_b	−18.91
x_{ss}	ϵ_{ss}	−12.17
x_{sb}^*	ϵ_{sb}	−19.12
λ	β_{12}	−112.96
λ'	λ'	6.04
λ''	λ''	−0.16
γ	β_{22}	−1.82
$\lvert k_{sbb}\rvert$	β_{sb}	18.79

[a]From Ref. 25.

[b]Most of the values are same except for β_{12}, β_{sb}, λ', λ'', and γ which reflect the correct classical limit of the quantum Hamiltonian in Ref. 25.

Table I shows the correspondence between parameters used here and Baggot's parameters.

III. CLASSICAL MECHANICS OF 3-MODE H_2O

In this section we examine the classical mechanics of the 3-mode Baggot vibrational H_2O Hamiltonian. The results of our analysis are summarized in Figure 1, which shows the classical phase space structure in the (I_1,I_2) plane for $\mathscr{N}=34.5$ ($\mathsf{P}=16$). Figure 1 shows contours of $\mathscr{H}_0$, the location of periodic orbits, resonance channels, and families of resonant 2-tori. Note that the physical region of the plot is that for which the inequality $I_1+I_2\leqslant 34.5$ is satisfied.

A. Periodic orbits and their bifurcations

In studying the phase space structure of H_2O, a first step is the determination of the primary *periodic orbits* (pos). For a 3-mode system with 2 linearly independent resonance coupling vectors, these pos can be located by finding the station-

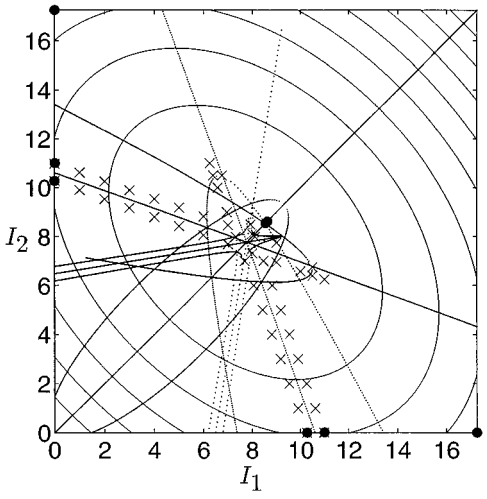

FIG. 1. Classical phase space structure of the Baggot Hamiltonian for H_2O. Primary periodic orbits (●) and resonant 2-tori (×) are shown. The multimode resonances are indicated by thin lines.

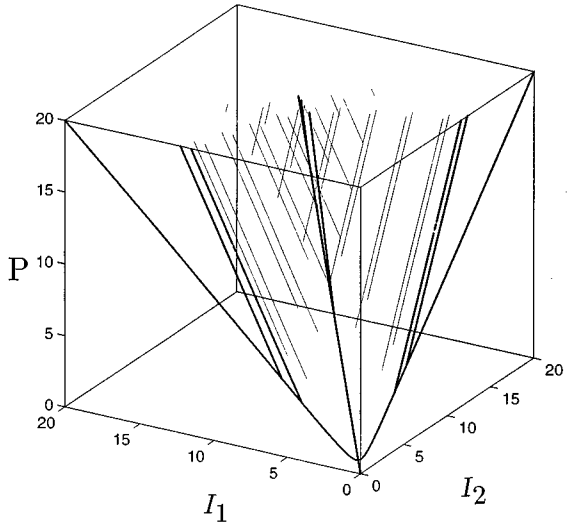

FIG. 2. Periodic orbit bifurcation diagram for the Baggot Hamiltonian in (P,I_1,I_2) space. The one parameter families of primary periodic orbits are shown as dark lines. The two parameter families of integrable limit 2:1 resonant 2-tori are shown as thin lines.

ary points of the effectively two-degree-of-freedom Hamiltonian expressed in terms of 2 resonant angles (cf. Appendix).

The primary pos appear in 1-parameter families in (P,I_1,I_2) space; the relevant bifurcation diagram has been computed by Lu and Kellman.[26] Following Lu and Kellman, we have determined the primary pos for the classical Baggot Hamiltonian (see Appendix). Figure 2 shows the families of periodic orbits and integrable limit 2-tori (see Section III C) in the $(\mathcal{N},I_1,I_2)$ space. For small values of $\mathcal{N}$ (P) there are three pos, which are the nonlinear normal modes whose existence is predicted by the Weinstein-Moser theorem.[53] The first bifurcation (pitchfork) leads to the creation of two local mode stretches. The local mode stretches undergo further bifurcations for larger $\mathcal{N}$ due to the 2:1 resonance interactions. The normal modes, meanwhile, also bifurcate due to the 2:1 resonance interaction with the bending mode. More important for the classical-quantum correspondence of the Baggot Hamiltonian in the manifold of quantum states studied here is the periodic orbit structure for a given value of $\mathcal{N}$.

The families of pos intersect constant $\mathcal{N}$ planes at *isolated points*, which are marked as circles in Figure 1. There are 3 pairs of symmetry related $(1\leftrightarrow 2)$ pairs of pos on the I_1 and I_2 axes, respectively (filled circles). Two are pairs of 2:1 bond stretch-bend pos, one stable and one (singly) unstable. The remaining pair consists of a pair of local mode stretch orbits, where all energy is in one or the other bond stretching mode. In addition, pos appear along the diagonal $I_1=I_2$. For example, for all values of $\mathcal{N}$ there are *two* pos with $I_1=I_2=\mathcal{N}/4$ (filled circle), corresponding to stable and unstable (asymmetric and symmetric stretch, respectively) normal mode pos. At $\mathcal{N}=34.5$, there are two other pos on the diagonal. One (filled circle) lies in the physical region of action space, and is a 2:1 bend/normal mode resonant po; another po lies outside the physical action region, and is also a bend/normal mode po.

We see that, for fixed $\mathcal{N}$, the primary pos appear at *isolated* points in the action plane. The probability of finding one of the primary pos at an arbitrary value of the classical energy is zero. The primary pos alone do not therefore form a ''skeleton'' for the classical phase space structure. To map out the classical phase space structure in a way that is useful for studying the classical-quantum correspondence it is necessary to consider higher dimensional classical objects; such objects are resonance channels, the object of standard Chirikov analysis, and families of resonant 2-tori.

B. Chirikov resonance analysis for $\mathscr{H}_0$

Resonance conditions for the Baggot Hamiltonian are determined in the usual way[27] by analyzing $\mathscr{H}_0$. Zeroth order frequencies are

$$\omega_\sigma \equiv \frac{\partial \mathscr{H}_0}{\partial I_\sigma} = \Omega_s + 2\alpha_s I_\sigma + \epsilon_{ss}(1-\delta_{\sigma\sigma'})I_{\sigma'} + \epsilon_{sb} I_b\,,$$

$$\sigma = 1,2, \tag{3.1a}$$

$$\omega_b \equiv \frac{\partial \mathscr{H}_0}{\partial I_b} = \Omega_b + 2\alpha_b I_b + \epsilon_{sb}\sum_{\sigma=1,2} I_\sigma\,. \tag{3.1b}$$

The resonance conditions for the 1:1 and 2:1 cases are obtained by setting $\omega_1(\mathbf{I})=\omega_2(\mathbf{I})$ and $\omega_\sigma(\mathbf{I})=2\omega_b(\mathbf{I})$, respectively, yielding immediately the resonance conditions in action space

$$2(\epsilon_{sb}-\alpha_s)I_\sigma + (2\epsilon_{sb}-\epsilon_{ss})I_{\sigma'}(1-\delta_{\sigma\sigma'}) = \Omega_s - 2\Omega_b + (\epsilon_{sb}-4\alpha_b)I_b\,, \tag{3.2a}$$

$$I_1 = I_2\,, \tag{3.2b}$$

for the 2:1 and 1:1 cases, respectively, with $\sigma,\sigma' = 1,2$.

Each of the resonance conditions defines a plane in the 3D action space. These planes intersect the constant $\mathcal{N}$ plane in a line, which defines the center of the resonance channel. All three resonance lines intersect at a point $\mathbf{I}^r$, which lies either inside or outside the physically allowed part of the action plane, $I_1+I_2 \lesseqgtr \mathcal{N}/2$, depending on the value of $\mathcal{N}$.

To estimate the resonance channel widths in action space consider the generating function

$$\mathscr{F} = \sum_{\sigma=1,2}\theta_\sigma I_\sigma^r + \theta_b I_b^r + \sum_{\sigma=1,2}(\theta_\sigma - 2\theta_b)J_\sigma + \left(A\theta_b + B\sum_{\sigma=1,2}\theta_\sigma\right)J, \tag{3.3}$$

which generates the canonical transformation $(\mathbf{I},\boldsymbol{\theta})\rightarrow(\mathbf{J},\boldsymbol{\psi}) \equiv (J_\sigma,\psi_\sigma,J,\psi)$ given by

$$\psi_\sigma = \theta_\sigma - 2\theta_b\,; \quad I_\sigma = I_\sigma^r + J_\sigma + BJ \tag{3.4a}$$

$$\psi = A\theta_b + B\sum_{\sigma=1,2}\theta_\sigma\,; \quad I_b = I_b^r + AJ - 2\sum_\sigma J_\sigma\,. \tag{3.4b}$$

Bilinear terms of the form $J_\sigma J$ in the new Hamiltonian can be eliminated by suitable choice of the parameters A and B. In terms of the new variables defined by the generating function $\mathcal{F}$, we transform our original Baggot Hamiltonian to a new Hamiltonian centered at $\mathbf{I}^r$:

$$\mathcal{H}\rightarrow\mathcal{H}_0(\mathbf{I}^r)+\tilde{c}\sum_{\sigma=1,2}J_\sigma^2+\tilde{c}_{12}J_1J_2+g(J)+\beta'_{12}[I_1(\mathbf{J})I_2(\mathbf{J})]^{1/2}\cos(\psi_1-\psi_2)+\sum_{\sigma=1,2}\beta_{\sigma b}[I_\sigma(\mathbf{J})I_b^2(\mathbf{J})]^{1/2}\cos\psi_\sigma, \tag{3.5}$$

where

$$\tilde{c}\equiv 4\alpha_b-2\epsilon_{sb}+\alpha_s, \tag{3.6a}$$

$$\tilde{c}_{12}\equiv 8\alpha_b-4\epsilon_{sb}+\epsilon_{ss}. \tag{3.6b}$$

The resulting Hamiltonian is cyclic in the angle ψ, so that the conjugate action variable J is conserved. Expressing the conserved action J in terms of the original set of action variables $\mathbf{I}$ leads to a constant of motion in addition to the total energy

$$\mathcal{N}=2\sum_{\sigma=1,2}I_\sigma+I_b, \tag{3.7}$$

which is the classical analog of (twice) the superpolyad quantum number P. Conservation of $\mathcal{N}$ means that we can follow the classical evolution of action variables for a given $(\mathcal{N},E)$ in the 2-dimensional action plane (I_1,I_2). Moreover, we can eliminate I_b to obtain equations for the resonance lines in terms of I_1 and I_2

$$I_2=\frac{\zeta}{\tilde{c}_{12}}-\frac{2\tilde{c}}{\tilde{c}_{12}}I_1, \tag{3.8a}$$

$$I_2=\frac{\zeta}{2\tilde{c}}-\frac{\tilde{c}_{12}}{2\tilde{c}}I_1, \tag{3.8b}$$

$$I_2=I_1, \tag{3.8c}$$

where $\zeta\equiv 2\Omega_b-\Omega_s+(4\alpha_b-\epsilon_{sb})\mathcal{N}$, and the location of the resonance intersection is given by

$$I_1^r=I_2^r=\frac{\zeta}{2\tilde{c}+\tilde{c}_{12}}. \tag{3.9}$$

In accordance with standard approximations,[27] we ignore the J_1J_2 coupling and assume that the coefficients of the resonance terms are slowly varying functions of $\mathbf{J}$. The latter assumption is reasonable in the vicinity of the resonance intersection point $\mathbf{I}^r$ and leads to the following resonant Hamiltonian:

$$\mathcal{H}^r\approx\tilde{c}\sum_{\sigma=1,2}J_\sigma^2+\beta'_{12}(I_1^rI_2^r)^{1/2}\cos(\psi_1-\psi_2)+\sum_{\sigma=1,2}\beta_{\sigma b}(I_\sigma^r)^{1/2}I_b^r\cos\psi_\sigma, \tag{3.10}$$

where $I_b^r=\mathcal{N}-2\Sigma_{\sigma=1,2}I_\sigma^r$. At this stage, averaging $\mathcal{H}^r$ over either ψ_1 or ψ_2 leads to a Hamiltonian of the familiar *pendular* form governing the motion of J_2 or J_1 respectively. Thus the resonance widths for the two 2:1 resonances at $\mathbf{I}^r$ are given by

$$\Delta I_\sigma^{2:1}\approx\left[\frac{8}{\tilde{c}}\beta_{\sigma b}(I_\sigma^r)^{1/2}I_b^r\right]^{1/2}. \tag{3.11}$$

The resonance width for the 1:1 channel can be estimated in a similar fashion by considering a further canonical transformation $(\mathbf{J},\boldsymbol{\psi})\rightarrow(\mathbf{K},\boldsymbol{\phi})$ generated by

$$\mathcal{G}(\mathbf{K},\boldsymbol{\psi})=\sum_{\sigma=1,2}\psi_\sigma J_\sigma^r+(\psi_1-\psi_2)K_1+(\psi_1+\psi_2)K_2, \tag{3.12}$$

and averaging the resultant Hamiltonian over the ϕ_2 variable. The resonance width is obtained as

$$\Delta I^{1:1}\approx\left[\frac{8}{2\tilde{c}-\tilde{c}_{12}}\beta'_{12}(I_1^rI_2^r)^{1/2}\right]^{1/2}. \tag{3.13}$$

Resonance widths at points along the resonance lines away from the intersection point $\mathbf{I}^r$ are determined, approximately, by substituting $\mathbf{I}^r\rightarrow\mathbf{I}$ in the above expressions for the widths (cf. Ref. 43). Thus we have approximately determined the location and extent of the relevant classical resonance channels. Note that, since $\beta_{12}<0$ and $\lambda'>0$, the 1:1 resonance width actually *decreases* as the actions I_1,I_2 get larger, i.e., for smaller values of the bend action I_b.

Resonance lines and corresponding channels are plotted in Figure 1. The diagonal $I_1=I_2$ is the 1:1 resonance line; in the absence of any other resonances, the region of phase space inside the associated resonance channel corresponds to normal mode trajectories, the region outside to local mode trajectories. The line $I_1+I_2=$const is then a projection of the polyad phase sphere for the 1:1 resonance (constant I_b) into the (I_1,I_2) plane. The two symmetry related 2:1 resonance zones slope inwards towards the 1:1 resonance zone. In the absence of other resonances, each 2:1 resonance channel is a region of phase space in which the bend mode and one of the local stretch modes are strongly coupled. The widths of the 2:1 resonance channels decrease to zero near the center of the action plane.

Of particular interest for the vibrational dynamics of the H_2O molecule are the regions of phase space where the primary resonance channels intersect. Such intersections are characteristic of the dynamics of multimode systems, giving rise to chaotic classical dynamics.[32,34] For $\mathcal{N}=18.5$ ($\mathsf{P}=8$), Chirikov resonance analysis shows that the primary resonance channels hardly intersect; consistent with this is the relative ease with which eigenstates for the $\mathsf{P}=8$ manifold can be assigned.[47]

Assignment of eigenstates for $\mathsf{P}=8$ has recently been considered by Rose and Kellman.[48] Eigenvalue correlation diagrams are used in the single resonance approximation to label each zeroth-order state as resonant or nonresonant with respect to stretch-stretch and stretch-bend couplings, respectively.[48] This ''schematic'' Chirikov-type analysis (cf. Figure 4 of Ref. 48) should be contrasted with the classical resonance analysis presented here, where the classical action

space is partitioned into resonance zones by explicit computations using the classical Baggot Hamiltonian.

In order to arrive at an unambiguous assignment of states, Rose and Kellman had to assume that normal mode classification (N-N-B in their notation) took precedence over local mode (L-L-B) assignment.[48] Moreover, it was noted that no states were assigned both normal mode (N-N-B) and Fermi resonant (L-R-R) labels. The explicit Chirikov analysis presented here and in Ref. 47 provides a clear dynamical justification for these empirical observations in terms of the location of the 1:1 and 2:1 classical resonance channels, especially the fact that for $\mathsf{P}=8$ the resonance zones do not overlap appreciably. On the other hand, for $\mathscr{N}=34.5$ ($\mathsf{P}=16$), the case studied here, three resonance channels intersect in the region around $I_1=I_2=8$. It is in this region of action space that ''mixed'' or nominally chaotic states are found (see below).

In addition to the primary 1:1 and 2:1 resonance zones, the location of higher-order multimode resonances can also be calculated at the next order of perturbation theory. In the Baggot Hamiltonian, Poincaré surfaces of section (discussed in section III D) show a particular multimode resonance occupying a significant region of phase space at energies below that at which the primary 2:1 resonance islands appear. Such multimode resonances arise due to the interaction between local modes and 1:1 resonant modes. They are indicated in Figure 1 as a pair of thin resonance zones. By Fourier analysis of classical trajectories located in the relevant region of phase space,[54,55] we have determined that these multimode resonances correspond to the (symmetry related) resonance vectors $(2,-1,-2)$ and $(-1,2,-2)$. We have also estimated the resonance width and location for the particular multimode resonance by removing the 1:1 resonance to first order[56] (see also Ref. 57). This calculation is the first step in a possible renormalization analysis[58] of higher order resonances, which could lead to an accurate determination of the threshold for onset of large-scale stochasticity. The widths of the corresponding multimode resonances are:

$$\Delta_m \approx \left[\frac{8\beta_{\sigma b}\beta_{12}}{\alpha_1(9\alpha_1+\alpha_2)}\,\frac{I_b I_{1,2}^{1/2}}{(I_1-I_2)}\right]^{1/2}, \tag{3.14}$$

where $\alpha_{1,2}\equiv 2\tilde{c}\mp\tilde{c}_{12}$. Note that this perturbative result does not hold as one approaches the resonance intersection $\mathbf{I}^r$ in the (I_1,I_2) plane.

C. Families of resonant 2-tori

Chirikov resonance analysis provides an approximate picture of the phase space structure of the H_2O molecule. It is a perturbative approach in that each resonance coupling term is analysed independently. Moreover, the phase space structure in the vicinity of each resonance line is assumed to be pendulum-like.[27] For systems with weak anharmonicities, there may be ranges of E and $\mathscr{N}$ over which the local phase space structure is more complicated.

A more detailed analysis of the phase space structure involves determination of the location of families of *resonant 2-tori*. Consider the classical H_2O Hamiltonian with a single resonance coupling term. There are in this case 2 ignorable angles, and 2 constants of the motion in addition to the energy; for example, if only the 1:1 resonance coupling term is present, I_b and I_1+I_2 are constants of the motion. The dynamics is then described by a 1 degree of freedom reduced Hamiltonian, and stationary (equilibrium) points of this Hamiltonian correspond to 2-tori in the full phase space. (In the absence of any coupling, almost all trajectories lie on nonresonant 3-tori.) Details of the computations of resonant 2:1 tori for the 1:1 and 2:1 resonances in the Baggot Hamiltonian are given in the Appendix.

At fixed superpolyad number $\mathscr{N}$, the resonant 2-tori appear in continuous one-parameter families, as shown in Figure 1 (two parameter families in $(\mathscr{N},I_1,I_2)$ space as shown in Figure 2). For the 1:1 resonant case, there are 2 families of normal mode 2-tori along the diagonal $I_1=I_2$, and a symmetry related pair of local mode 2-tori along the I_1 and I_2 axes. In addition, there are two families of resonant 2-tori associated with bend-local resonant motion; these families are marked with crosses in Figure 1, and are located close to the centers of the 2:1 resonance channels determined via Chirikov analysis. We stress again that our computations of the resonant 2-tori are not exact, but are carried out within the single resonance approximation.

Two conclusions are evident from our computation of the resonant 2-tori. First, from Figure 2 it is clear that the primary pos appear where families of 2-tori meet. Moreover, the location of the primary pos is given quite accurately by the intersection of the loci of the families of 2-tori determined in the single-resonance approximation. Second, it is apparent that the 2-tori form the ''skeleton'' of the classical phase space, and in fact follow very closely the Chirikov resonance channels. All this suggests that the Chirikov analysis is meaningful for the Baggot Hamiltonian.

D. Poincaré surface of section

In addition to the calculations outlined above, we have computed classical surfaces of section for the Baggot Hamiltonian. These surfaces of section are useful in order to determine the significance of the classical phase space structures discussed above, and also to compare with quantum mechanical phase space (Husimi) distribution functions.

As the Baggot Hamiltonian has one ignorable angle, we can define a 2D surface of section (sos) by plotting $N_1\equiv(I_1-I_2)/2$ and $\phi_1\equiv\theta_1-\theta_2$ at constant values of the sectioning angle $\phi_2\equiv\theta_1+\theta_2-4\theta_b$ with $\dot{\phi}_2>0$. The value of the ignorable angle conjugate to the superpolyad action ($\mathscr{N}$) is irrelevant. All trajectories in a given sos have the same energy E; for given $\mathscr{N}$ there is a range of possible sos energies.

The general structure of the classical sos is as follows: a normal-mode resonant region is present in the middle of the sos ($I_1\simeq I_2$), corresponding to ''librational'' motion.[5] Local mode (above barrier) regions are found above and below the central normal mode region. Large 2:1 bend/local-stretch resonant islands appear in the local mode regions (e.g., Figure 3b). Higher-order resonances also appear. At low ener-

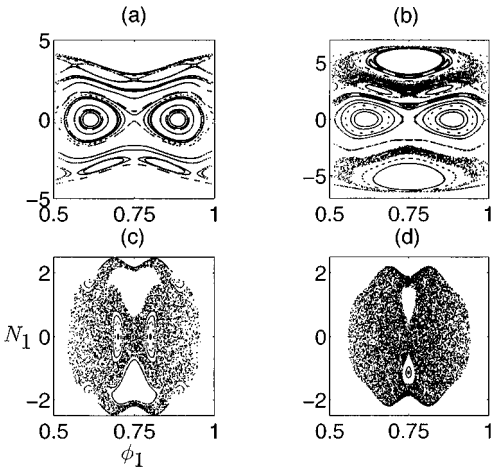

FIG. 3. Lower Poincaré surface of sections for P=16 as a function of increasing energy. (a) 41892 cm^{-1}. (b) 43488 cm^{-1}. (c) 48970 cm^{-1}. (d) 49157 cm^{-1}.

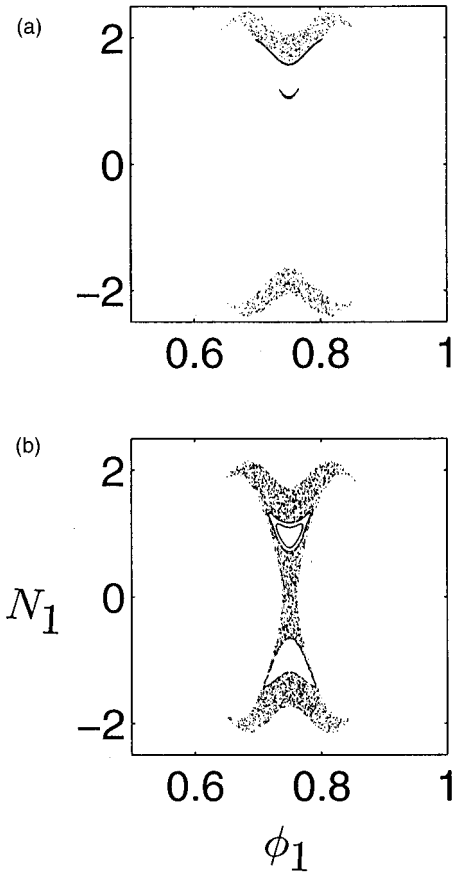

FIG. 4. Poincaré surfaces of section for P=16 at energies corresponding to Figure 3. (a) 48970 cm^{-1}. (b) 49157 cm^{-1}.

gies, the center of the normal mode islands correspond to stable resonant 2-tori, while a ''whiskered'' (unstable) 2-torus appears at the center of the sos. Similarly, the 2:1 bend/local-stretch resonance is defined by the intersection of stable and unstable resonant 2-tori with the sos.

The classical surface of section described above has an additional feature which manifests itself at values of the superpolyad number for which the resonance intersection $\mathbf{I}^r$ lies in the physical region of the action plane. This feature is an apparently unavoidable ''double-sheetedness'' of the surface of section due to the closing of the contours of $\mathscr{H}_0$ around $\mathbf{I}^r$ (cf. Figure 1). Such a topological change in the contours of $\mathscr{H}_0$, and thence of the phase space of the effective 2D reduced system, leads to the possibility of the creation/destruction of fixed points in phase space, as follows in general from the analysis of stratified Morse theories.[13] An interesting aspect of the two-sheeted structure of the surface of section is that some quantum states can selectively localize on one sheet or the other whilst other states can delocalize over both sheets. Examples of such states are shown and discussed below. Moreover, interaction between such states can lead to very highly mixed states, thus complicating the spectral assignments.

In our calculations points on the classical sos are determined to lie on the upper or lower sos via a simple criterion. The value of the bend action (I_b^r) corresponding to the resonance intersection is obtained as $I_b^r = \mathscr{N} - 2(I_1^r + I_2^r)$. The intersection point of the classical trajectory with the sos lies on the lower or upper sos if the associated value of I_b is less than or greater than I_b^r, respectively. In what follows, both sheets of the surface of section are shown (when necessary) with u and l denoting upper and lower sheets respectively. All (N_1, ϕ_1) surface of sections shown in this paper correspond to the angle ϕ_1 measured in units of 8π.

In Figure 3 a series of 4 surfaces of section are shown (N_1 versus $\phi_1/8\pi$) as a function of increasing energy for P $=16$. At low energies (Figure 3a) most of the surface of section is occupied by regular normal mode orbits, together with large islands corresponding to the $(2,-1,-2)$ and $(-1,2,-2)$ multimode resonances as discussed in the previous section (cf. section III B). At moderate energies (Figure 3b), the main features are the 2:1 and 1:1 islands with the destruction of the multimode resonances. Although there is increased stochasticity due to the higher order resonances, there are still invariant curves serving as barriers to transport in phase space. In Figure 3c the surface of section corresponds to energies close to that of the bifurcation of the normal mode periodic orbits due to the 2:1 resonances. At these high energies, most of the sos is occupied by stochastic orbits with the relatively small 2:1 islands embedded in the stochastic sea. The islands do not have enough phase space area to support even a single quantum state. At even higher energies as shown in Figure 3d the entire sos is filled with stochastic orbits. The 1:1 regions are completely destroyed with small islands of 2:1 resonances still persisting. At the highest energy almost all of the invariant curves in the sos are destroyed in marked contrast to the analogous case for P $=8$.

The surfaces of section shown in Figures 3c and 3d are at high enough energy so that the sos is double-sheeted; in Figure 4 we show the corresponding upper sos. At the highest energies all of the invariant structures on the upper sos are also destroyed.

IV. ANALYSIS OF EIGENSTATES: METHODS

Quantum eigenfunctions were generated by diagonalizing the Baggot Hamiltonian for a given polyad number P in the number basis $|n_1,n_2,n_b\rangle$, where n_1,n_2 are the quantum numbers for the anharmonic local O-H stretch modes and n_b denotes the bend quantum number. The Hamiltonian is block diagonal in P and the total number of states at fixed P is $(P+1)(P+2)/2$. To analyze the eigenstates of the Baggot Hamiltonian, it is natural to project them onto the (n_1,n_2) quantum number (action) plane. The physical points in the (n_1,n_2) lattice are those points for which $P-n_1-n_2$ is nonnegative. We represent the eigenstates by plotting at every physical lattice point a circle with radius equal to the square of the coefficient of the corresponding zeroth-order basis state in the eigenstate of interest. In the present paper, we discuss the manifold of 153 states with $P=16$. Analysis of the case $P=8$ has been presented in an earlier paper.[47] In the rest of this section we give a brief description of the methods used for studying the classical-quantum correspondence.

A. Inverse participation ratios (IPR)

To analyze the quantum wavefunctions, and to aid in correlating with the classical resonance analysis, we have computed inverse participation ratios (IPR) for eigenstates.[49] If the state $|\Psi_\alpha\rangle$ is expanded in an orthonormal basis $\{\phi_j\}$ as

$$|\Psi_\alpha\rangle=\sum_j |\phi_j\rangle c_{j\alpha}, \tag{4.1}$$

then the corresponding IPR is defined by

$$L_\alpha=\sum_j |c_{j\alpha}|^4. \tag{4.2}$$

The IPR is a measure of the delocalization of $|\Psi_\alpha\rangle$ in the basis $\{\phi_j\}$: if $|\Psi_\alpha\rangle$ is essentially composed of a single basis state, then the IPR will be about unity; on the other hand, if $|\Psi_\alpha\rangle$ is a superposition of N basis functions with comparable coefficients, then the value IPR will be about $1/N$. States with low IPR values are therefore delocalized over the basis $\{\phi_j\}$.

The value of the IPR is of course by definition basis set dependent. In addition to obtaining a rough measure of eigenstate delocalization, we are interested in using IPRs calculated in terms of one or more physically appropriate basis sets to distinguish between different classes of eigenstate. Following the analysis by Atkins and Logan of a 3-mode system with two resonant coupling terms,[43] we compute the IPR in two different basis and average over them. In our case, we compute the IPR in a basis of eigenfunctions of the zeroth-order Hamiltonian plus the 1:1 resonant coupling term, and in the basis of eigenstates of $\mathscr{H}_0$ plus *both* 2:1 resonant coupling terms. We then calculate an average IPR defined by

$$\mathsf{L}=\frac{1}{2}(L_{1:1}+L_{2:1}), \tag{4.3}$$

where

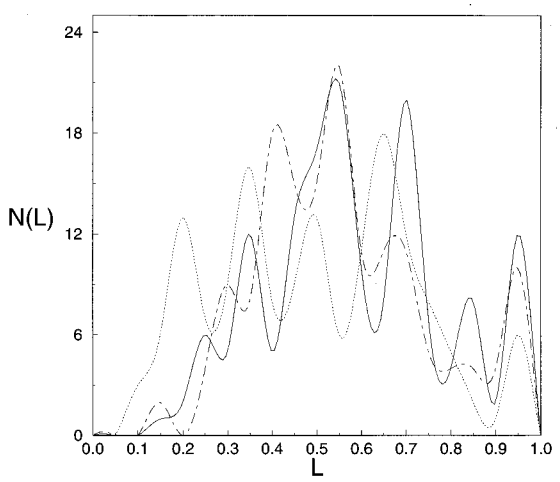

FIG. 5. Smoothed histogram of average IPRs, L, for the full Baggot Hamiltonian (solid), $\lambda'=0$ (dotted), and $\beta_{22}=0$ (dashed). $P=16$.

$$L_{1:1}=\sum_j |c_{j\alpha}^{1:1}|^4,$$
$$L_{2:1}=\sum_j |c_{j\alpha}^{2:1}|^4. \tag{4.4}$$

Here, $c_{j\alpha}^{1:1}$ and $c_{j\alpha}^{2:1}$ are the coefficients in the expansion of the eigenfunctions $|\Psi_\alpha\rangle$ in the 1:1 and 2:1 resonance bases, respectively. It follows from the definition of the IPR that states with mostly 1:1 resonant character will have high values of $L_{1:1}$ and low values of $L_{2:1}$ and vice versa. Strongly mixed states influenced by both 1:1 and 2:1 resonances are expected to have low values of the IPR in both bases. On the other hand, states that are completely outside either of the resonance zones will have the highest values of the IPR in both bases. Thus we provisionally associate low values of the average IPR, L, with mixed states, moderate values with states being in either the 1:1 or both of the 2:1 resonance zones and high values with states outside the influence of any of the resonance zones.

Note that, with our present definitions, low values of L should only be found for states that are strongly mixed by *all* resonant coupling terms. Thus, states that are mixed predominantly by the two 2:1 resonances, and which might be in some sense ''chaotic'' in the semiclassical limit (as the corresponding 2-resonance classical system is nonintegrable) will nevertheless have high values of $L_{2:1}$.

Figure 5 summarizes our IPR computations for the full Baggot Hamiltonian (all coupling terms included) with $\mathscr{N}=32$. The results are displayed as a smoothed histogram showing the number of states within a given range of L. It is apparent from the histogram that the IPR values do not yield a clean separation of eigenstates into 3 classes: nonresonant, singly-resonant and mixed, as they do for the case studied by Atkins and Logan.[43] The IPR appears to be too crude an indicator of eigenstate delocalization to provide a basis for classification of eigenstates of the Baggot Hamiltonian.

Also shown in the Figure 5 are the effects of setting coupling parameters λ' and γ to zero. The number of states

with very low values of the IPR increases sharply when λ' is set equal to zero, indicating a significant increase in mixing of zeroth-order states; Baggot[25] has stressed the importance of the parameter λ'. If the 2:2 resonant coupling term is removed by setting $\gamma=0$, however, there is only a minor change in the form of the histogram.

B. Husimi distribution functions

In order to explore the quantum-classical correspondence for the Baggot Hamiltonian in more detail, and to provide a dynamical basis for assignment of eigenstates, it is useful to have a *phase space* representation of the quantum wavefunctions; such a representation facilitates comparison of the structure of the quantum state with the important classical phase space structures.[9] Two well known representations are the Wigner[59] and the Husimi[50] functions. We use the Husimi representation since the Wigner representation can take negative values, thereby invalidating its use as a probability distribution, and also exhibits oscillations on a finer and finer scale as $\hbar\rightarrow 0$.[59] The Husimi function is a Gaussian smoothed version of the Wigner function. It is nonnegative, and is well suited for study of the classical-quantum correspondence.[60] Other related approaches to the definition of quantum phase space involve the construction of generalized coherent states[61] which take into account the underlying dynamical symmetry group of the problem. For present purposes, however, we use the following simple method to obtain the necessary distribution function.

We start by laying down a grid in the (N_1,ϕ_1) coordinates on the Poincaré surface of section (i.e., for a fixed value of the sectioning angle $\phi_2=\phi_2$). For a given point on this grid, denoted by $(N_1^{(k)},\phi_1^{(k)})$, and the chosen value of ϕ_2, we calculate the associated values of the original canonical variables $(\mathbf{I}^{(k)},\boldsymbol{\theta}^{(k)})$. To compute $(\mathbf{I}^{(k)},\boldsymbol{\theta}^{(k)})$ we must pick an arbitrary value (equal to zero for results reported in this paper) of the ignorable angle ψ conjugate to the superpolyad action J, and ensure that the energy of the classical phase space point equals that of the eigenstate under consideration. Cartesian coordinates $(p_\mu^{(k)},q_\mu^{(k)})$, $\mu=1,2,b$, associated with the grid point $(N_1^{(k)},\phi_1^{(k)})$ are then calculated via the usual harmonic action-angle transformations. The value of the Husimi function for eigenstate $|\Psi\rangle$ at phase space point $(\mathbf{p}^{(k)},\mathbf{q}^{(k)})$ is calculated by taking the square of the overlap of $|\Psi\rangle$ with a product of minimum uncertainity Gaussians

$$\chi(q_\mu)=\left(\frac{c_\mu^2}{\pi}\right)^{1/4}\exp\left[-\frac{c_\mu^2}{2}(q_\mu-q_\mu^{(k)})^2+\frac{i}{\hbar}p_\mu^{(k)}q_\mu\right], \tag{4.5}$$

for each of the three modes $\mu=1,2,b$. Diagonalization of the Baggot Hamiltonian in a number basis gives the eigenstates $|\Psi\rangle$ as linear combinations of a finite number of products of harmonic oscillator basis functions $\varphi_{n_\mu}(q_\mu)$:

$$\Psi(\mathbf{q}_\mu)=\sum_{n_1n_2n_b}C_{n_1n_2n_b}\varphi_{n_1}(q_1)\varphi_{n_2}(q_2)\varphi_{n_b}(q_b). \tag{4.6}$$

The resulting Gaussian integrals are performed analytically to give the Husimi distribution function as $|\mathsf{A}|^2$, where

$$\mathsf{A}(p^{(k)},q^{(k)})=\sum_{n_1n_2n_b}\mathsf{C}_{n_1n_2n_b}\prod\frac{1}{\sqrt{n_\mu}}\zeta_\mu^{n_\mu}\times\exp\left[-\frac{1}{2}|\zeta_\mu|^2+\frac{i}{2\hbar}p_\mu^{(k)}q_\mu^{(k)}\right]. \tag{4.7}$$

In the above equation we have defined

$$\zeta_\mu\equiv\frac{c_\mu}{\sqrt{2}}q_\mu^{(k)}+\frac{i}{c_\mu\hbar\sqrt{2}}p_\mu^{(k)}, \tag{4.8}$$

with c_μ^2 the mode harmonic frequencies.

Note that the Husimi functions need only be computed for one quadrant of the (N_1,ϕ_1) surface of section due to the symmetry of the full Baggot Hamiltonian. To explore the classical-quantum correspondence for eigenstates, contours of the Husimi distribution functions are superimposed on the classical surface of section at an energy corresponding that the particular quantum state. In computing the Husimi functions contributions from both upper and lower sheets of the sos (when present) are added incoherently.

V. BAGGOT HAMILTONIAN: SPECIAL CASES

Before tackling the full Baggot Hamiltonian, it is useful to examine eigenstates of Hamiltonians obtained by keeping only selected resonant coupling terms (see also Ref. 48). In the case that a single resonant coupling term is present, the Hamiltonian is classically completely integrable. When two resonant coupling terms are present (e.g., 1:1 plus 2:1, or both 2:1 terms), the Hamiltonian is nonintegrable, but possesses a constant of the motion in addition to the energy. This constant of the motion persists in the Baggot Hamiltonian when all three coupling terms are present, as the three resonance vectors are linearly dependent.[51]

A. $\mathscr{H}_0$ plus a single 2:1 stretch-bend resonance

Figure 6 shows projections onto the action lattice of several eigenstates of the quantum Hamiltonian obtained by adding a single 2:1 stretch-bend coupling term to $\mathscr{H}_0$. The eigenstates are superimposed upon a plot of the 2:1 resonance zone in the (I_1,I_2) action plane. In action space, the eigenstates are delocalized along the line $n_2=\text{const}$, i.e., $\mathscr{N}_{1b}\equiv 2n_1+n_b$ is conserved in accord with the classical behavior of the action variables for a single 2:1 resonance.

Figure 6 shows action projections for a sequence of states at constant n_2, corresponding to increasing excitation transverse to the resonance channel. A precise dynamically based assignment of these eigenstates is obtained by examining associated Husimi functions: for resonant states, the quantum phase space density is localized inside the relevant resonance channel in the surface of section, whereas for nonresonant states the quantum phase space density lies outside (''separatrix'' states[62] occur at the boundary between the 2 classes of state, and have phase space density localized on unstable objects [fixed points] in the surface of section). Each resonant state can be assigned three quantum numbers: $\langle\mathscr{N},\mathscr{N}_{\sigma b},\nu\rangle$, where the quantum number $\nu=0,1,2\ldots$, measures the degree of excitation within the resonance. For ex-

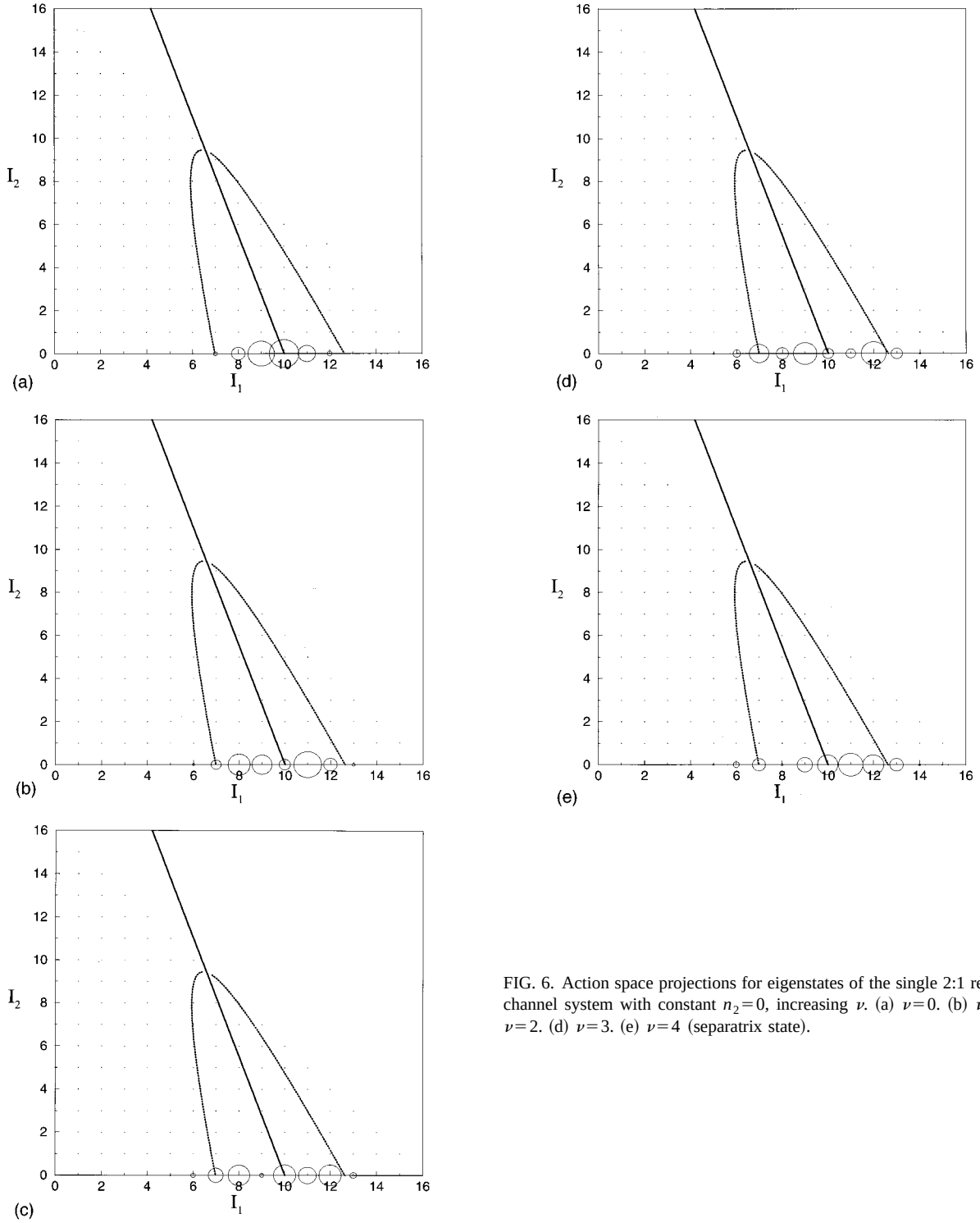

FIG. 6. Action space projections for eigenstates of the single 2:1 resonance channel system with constant $n_2=0$, increasing ν. (a) $\nu=0$. (b) $\nu=1$. (c) $\nu=2$. (d) $\nu=3$. (e) $\nu=4$ (separatrix state).

ample, for the sequence of resonant states shown in Figure 6, there are five resonant states with $\langle \mathcal{N}=32,\ \mathcal{N}_{1b}=32,\ \nu=0,1,2,3,4\rangle$. Note that the state with $\nu=4$ is a separatrix state. The associated Husimi distribution functions are shown in Figure 7. Note the movement of the maxima of the Husimi distributions outwards from the center of the resonance as one increases the excitation, with the final state clearly localized about the unstable 2-torus.

Nonresonant states, whose phase space density lies outside the classical resonance channel, can be assigned zeroth-order quantum numbers $(\mathcal{N},n_1,n_2)$, corresponding to the dominant zeroth-order state contributing to the eigenstate.

Our set of resonant quantum numbers $\langle \mathcal{N},\mathcal{N}_{\sigma,b},\nu\rangle$ for the integrable 2:1 case is closely related to that used by Rose and Kellman for L-R-R states: n_l, $\{n_{R1},n_{R2}\}$.[48] The superpolyad quantum number is $\mathcal{N}=2n_l+2n_{R1}+2n_{R2}$, the 2:1

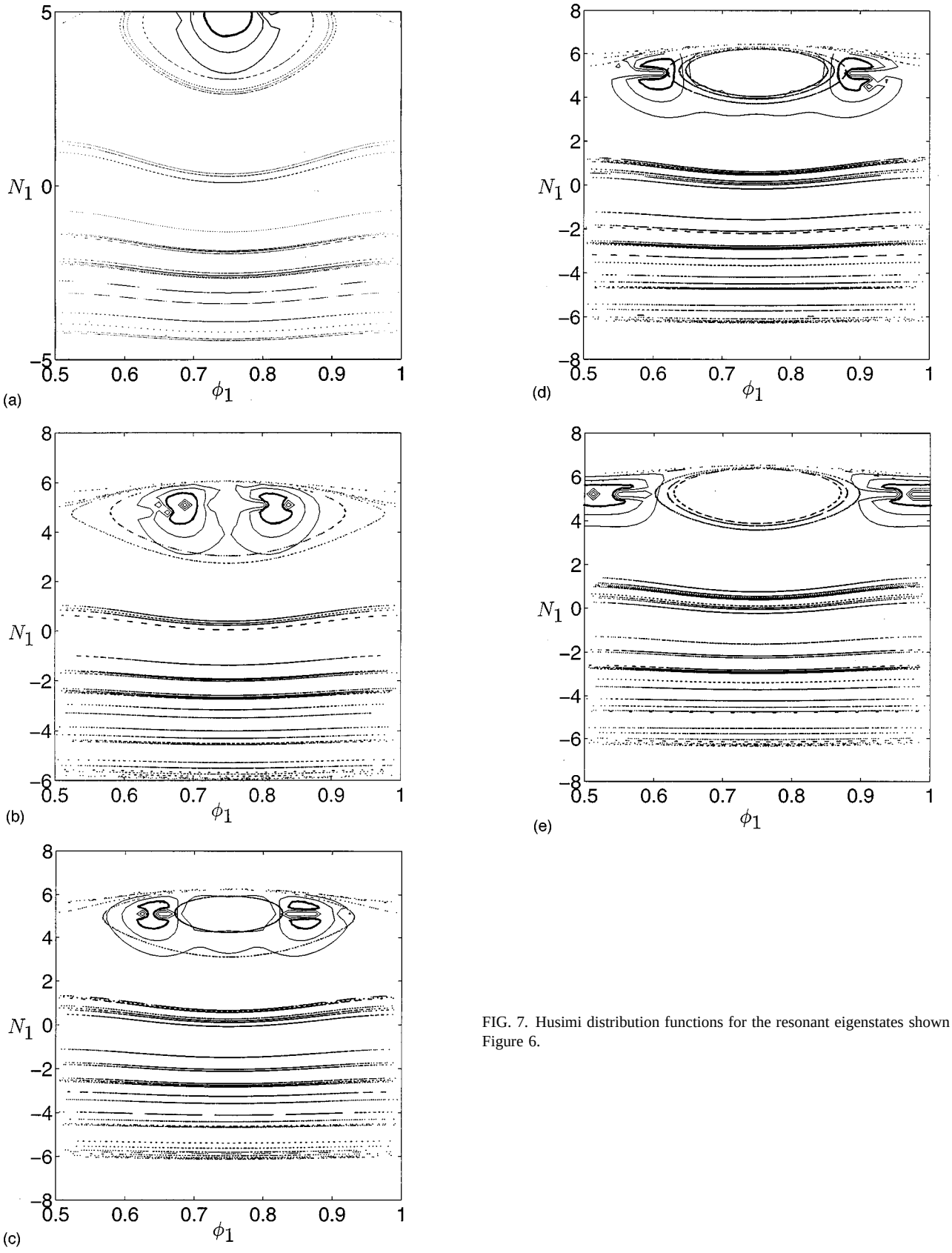

FIG. 7. Husimi distribution functions for the resonant eigenstates shown in Figure 6.

resonance quantum number is $n_{\sigma,b}=2n_{R1}+n_{R2}$, while the quantum number ν can presumably be identified with n_{R1}.

There has been much discussion in the literature concerning the correspondence between classical and quantum resonances (see, for example Ref. 63). The 2:1 stretch-bend resonance channel studied here is large and contains many states (as does the 1:1 resonance). The situation is therefore analogous to that studied by Ramchandran and Kay, who

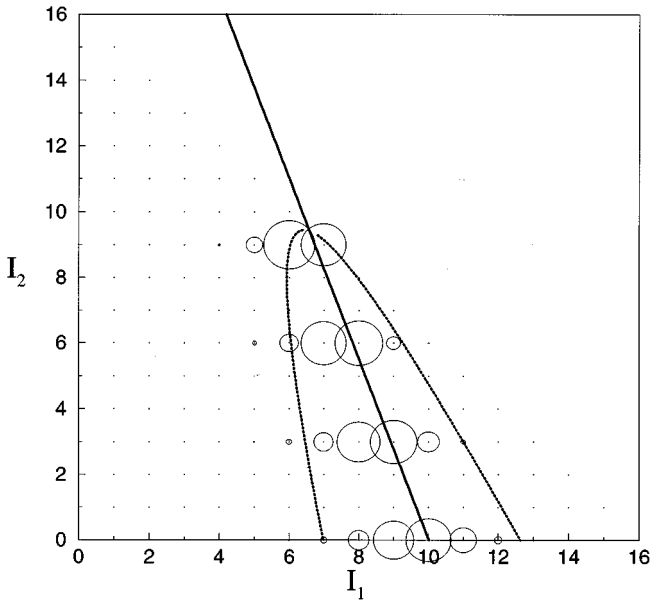

FIG. 8. Action space projections for a sequence of eigenstates in the single 2:1 resonance system with constant $\nu=0$ and $n_2=0,3,6,9$.

examined the connection between the existence of avoided level crossings and classical resonant dynamics.[64] Conceptual problems concerning the classical-quantum correspondence for narrow, high-order resonances (width of order $\hbar$) have been discussed by Roberts and Jaffé.[45] In particular, these authors define quantum resonant eigenstates as those formed by strong interaction between zeroth-order states that may lie outside the (narrow) classical resonance channel.[45] From our perspective, such states have (distorted but) topologically nonresonant phase space densities (see, for example, Figure 2d of Ref. 47).

States localized in the 2:1 resonance channel with different values of n_2 form sequences, where each sequence is characterized by a particular value of the excitation quantum number ν. In Figure 8 we show a sequence of states which progresses along the 2:1 resonance zone. The 4 states in Figure 8, for example, are assigned quantum numbers $\langle \mathcal{N}=32, \mathcal{N}_{1b}=32, \nu=0\rangle$, $\langle 32,26,0\rangle$, $\langle 32,20,0\rangle$ and $\langle 32,14,0\rangle$, respectively. The Husimi distributions for the above sequence of states are all localized in the vicinity of a stable resonant 2-torus (cf. Figure 7a).

We shall investigate below the fate of these eigenstates as the remaining resonant coupling terms are turned on.

An important observation is that n_1/n_b resonant states with similar distributions of amplitudes over the resonant region of action space, and the same value of ν, appear at intervals of $\Delta I_2=3$ in the action I_2 (cf. Figure 8). This periodicity is simply a consequence of the fact that the slope of the resonance line in the action plane is nearly -3; hence, the form of the stretch-bend Hamiltonian in the zeroth-order basis near the center of the resonance zone is approximately invariant as $n_2 \rightarrow n_2+3$.[65] The periodicity persists even upon inclusion of additional resonant couplings.

The size of the interval $\Delta n_2=3$ is an accidental consequence of the particular parameter values in our Hamiltonian. For example, if we set $\epsilon_{ss}=\epsilon_{sb}=0$ then the observed periodicity is $\Delta n_2=2$. In each case, however, the apparent periodicity in the location of isomorphic resonance states can be understood in terms of the slope of the classical resonance line. An analysis based solely on the properties of primary periodic orbits is, as far as we can see, unable to provide a comparably simple explanation of these relatively subtle properties of the eigenstate densities in action space.

To clarify the significance of the periodicity associated with the slope of the resonance line in the I_1, I_2 action plane, consider a simple, integrable Fermi resonant 2-mode Hamiltonian,

$$H=\Omega_\sigma I_\sigma+\Omega_b I_b+\alpha_\sigma I_\sigma^2+\epsilon_{sb} I_\sigma I_b+\alpha_b I_b^2 + \beta_{12} I_b I_\sigma^{1/2} \cos(\theta_\sigma-2\theta_b), \tag{5.1}$$

with $\sigma=1$ or 2. This Hamiltonian describes an integrable subsystem of the Baggot Hamiltonian. The resonance line in (I_σ, I_b) space is found by setting the frequency ratio equal to 2, $\omega_\sigma=2\omega_b$. This equation may be written:

$$I_b=\wp(I_\sigma-\mathcal{I}_\sigma), \tag{5.2}$$

where

$$\wp \equiv \frac{2(\epsilon_{sb}-\alpha_\sigma)}{(\epsilon_{sb}-4\alpha_b)}, \tag{5.3}$$

and

$$\mathcal{I}_\sigma \equiv \frac{(\Omega_\sigma-2\Omega_b)}{2(\epsilon_{sb}-\alpha_\sigma)}, \tag{5.4}$$

denote the periodicity and one of the intercepts of the resonance line, respectively. The phase space structure of this Hamiltonian has been studied in some detail including periodic orbit bifurcations[66] and the quantum (E,τ) characterization of the energy spectrum.[67] Performing a canonical transformation $(I_\sigma, I_b, \theta_\sigma, \theta_b) \rightarrow (I_z, \psi; I, \Psi)$ (Refs. 66, 67) and using the variables

$$Q=2\alpha_\sigma-8\alpha_b, \tag{5.5a}$$

$$\gamma_1=\alpha_\sigma+4\alpha_b+2\epsilon_{sb}, \tag{5.5b}$$

$$\gamma_2=\alpha_\sigma+4\alpha_b-2\epsilon_{sb}, \tag{5.5c}$$

$$P=\Omega_\sigma-2\Omega_b, \tag{5.5d}$$

it follows that the primitive periodic orbits (apart from the ones at North and South poles on the polyad phase sphere) can be obtained from the cubic equation:

$$Z^3 \pm e_1 Z^2 + e_2 Z \mp e_3 = 0. \tag{5.6}$$

In the above equation we have defined $Z \equiv (I+I_z)^{1/2}$ and

$$e_1=\frac{6\beta_{sb}}{2^{3/2}\gamma_2}, \tag{5.7a}$$

$$e_2=\frac{P+(Q-2\gamma_2)I}{2\gamma_2}, \tag{5.7b}$$

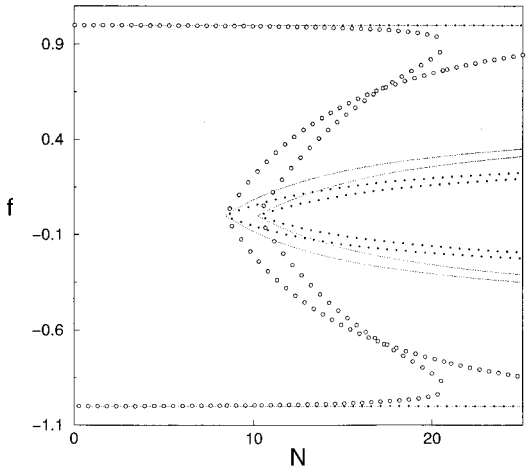

FIG. 9. Bifurcation diagram ($f \equiv \cos[(I_z - I)/2I]$ versus $\mathscr{N}$) as a function of the periodicity $\wp$ of the single 2:1 resonance line with fixed $\mathscr{T}_\sigma$, K_2. Physical (solid line), reduced $\wp$ (solid dots) and zero anharmonicity of bend mode (open circles).

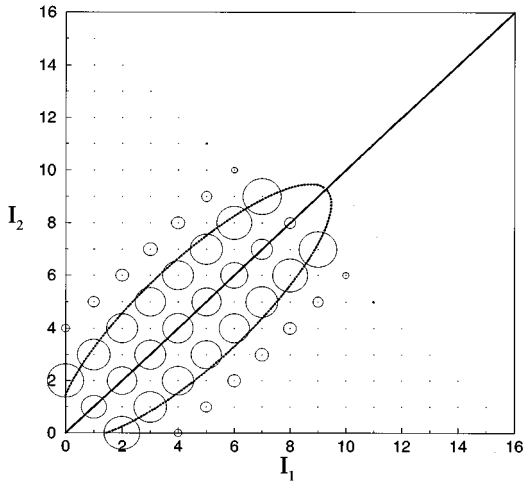

FIG. 10. Action space projections for a sequence of 1:1 resonant (normal mode) states for the 1:1+2:2 integrable subsystem and P=16.

$$e_3 = \frac{2\beta_{sb} I}{2^{1/2}\gamma_2}. \tag{5.7c}$$

One can express the coefficients of the cubic equation in terms of the variables $(\wp, \mathscr{T}_\sigma, P)$ using the following relations:

$$Q = \frac{(2-\wp)}{\wp \mathscr{T}_\sigma} P, \tag{5.8}$$

$$\gamma_2 = -\frac{(2+\wp)}{2\wp \mathscr{T}_\sigma} P. \tag{5.9}$$

We now study the evolution of the bifurcation diagram with varying $\wp$ and keeping $\mathscr{T}_\sigma$ constant. Contact with the Baggot Hamiltonian studied in this paper is made by replacing P by $P' \equiv P + (\epsilon_{ss} - 2\epsilon_{sb})K_2$, where K_2 is the conserved action corresponding to the nonresonant stretch mode. The superpolyad number for the Baggot Hamiltonian is related to the Fermi resonant polyad and K_2 through $\mathscr{N} = 4I + 2K_2$. Figure 9 shows the bifurcation plot ($f \equiv \cos\psi(I_z - I)/2I$ versus $\mathscr{N}$, with $\psi = 0, \pi$) as one varies the periodicity $\wp$ for fixed value of $\mathscr{T}_\sigma$ and K_2. For the physical value of $\wp$ (solid line), we have three roots for $\mathscr{N}$ greater than 12, signaling the presence of pendular resonance regions in phase space.[67] The three roots correspond to a local mode (stable) 2-torus and a pair of stable/unstable 2:1 resonant 2-tori, in agreement with our analysis of the 2-tori of the integrable subsystem given earlier (cf. also Appendix). On reducing $\wp$ by half (dots) we are still in the Chirikov regime. For the particular choice of Baggot parameters the periodicity $\wp > 0$ in the (I_σ, I_b) plane. Eliminating the bend anharmonicity, i.e., setting $\alpha_b = 0$ in the Baggot Hamiltonian leads to a different bifurcation structure as shown in Figure 9 (filled circles). Now one clearly sees values of $\mathscr{N}$ for which there are fewer than three roots and hence a non-pendular phase space. Quantum eigenfunctions for reduced bend anharmonicity are strongly mixed and bear little resemblance to the eigenstates analysed in this paper.

B. $\mathscr{H}_0$ plus the 1:1 and 2:2 stretch-stretch resonances

The Hamiltonian consisting of $\mathscr{H}_0$ plus the 1:1 and 2:2 stretch-stretch resonant coupling terms is also completely integrable. Eigenstates are delocalized along the line $n_1 + n_2 = \text{const}$. Just as for the 2:1 resonance, we can classify the 1:1 states as resonant or nonresonant according to whether the phase space densities are localized inside or outside the 1:1 resonance channel. States outside the 1:1 resonance zone can be assigned zeroth-order local mode quantum numbers $(\mathscr{N}, n_1, n_2)$. The line $n_1 + n_2 = \text{const}$ is the projection into the action plane of the polyad phase sphere for 1:1 resonant systems studied by Kellman and coworkers.[20] We note that the width of the 1:1 resonance decreases at higher values of $I_1 = I_2$.

Figure 10 shows a sequence of 1:1 resonant (normal mode, separatrix) states which progress along the 1:1 resonance channel and can be assigned resonant (normal mode) quantum numbers: $[n_b, \mathscr{N}_{12} = n_1 + n_2, \nu]$. The particular sequence shown in Figure 10 can be assigned as $[4k, 2l, 2]$ with $k = 0,1,\ldots,7$ and $l = 8 - k$. (The correspondence with the 1:1 resonant N-N-B quantum numbers of Rose and Kellman[48] is as follows: $\mathscr{N}_{12} = n_s + n_a$, $\nu = n_s$.)

Isomorphic normal mode states appear along the 1:1 resonance zone at intervals $\Delta\mathscr{N}_{12} = 2$, where all states in a given sequence have either a node or an antinode along the diagonal. This well known alternation can be viewed as a consequence of the slope $+1$ of the 1:1 resonance line. Figure 11 shows 4 of the corresponding Husimi distribution functions. The Husimi functions are all localized around the unstable normal mode 2-torus. The characteristic x-shape of Husimis localized in the vicinity of an unstable fixed point[60] is clearly evident in Figures 11c, 11d. The effect of the weak 2:2 resonance can be clearly seen in Figure 11d. Bifurcations

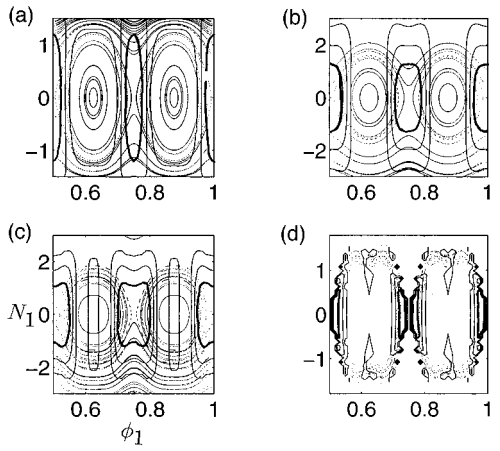

FIG. 11. Husimi distribution functions for the normal mode sequence with $\nu=2$ shown in Figure 10.

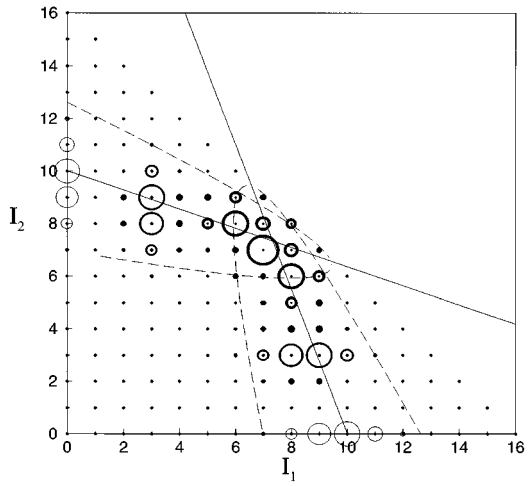

FIG. 12. Sequence of action space projections for eigenstates of two 2:1 resonance channel Hamiltonian with $\nu=0$ and $\mathcal{N}=32$. In order to distinguish the states in a sequence we plot them with different line thicknesses. Terminal states have the thickest line, and the same holds for all multiresonance action space plots shown in the rest of the paper.

occur which affect the topology of phase space and the corresponding Husimi distributions. Although we have not investigated the possible bifurcations in this subsystem in full detail, we note that the form of the Husimi distribution in Figure 11d is consistent with a bifurcation in the underlying classical surface of section.

C. $\mathscr{H}_0$ plus two 2:1 stretch-bend resonant coupling terms

The Hamiltonian consisting of $\mathscr{H}_0$ plus two 2:1 resonant coupling terms is classically nonintegrable. It nevertheless conserves the quantity $\mathcal{N}=2(n_1+n_2)+n_b$. In the rest of the figures involving action space projections for sequences of eigenstates we show the different states with varying thickness. The terminal state is shown with the largest thickness in the figures.

We now show action space projections for 3 sequences of eigenstates that progress along the 2:1 resonance channel. For example, in Figure 12 we show a sequence of states with $\nu=0$ and symmetric with respect to reflection in the diagonal $I_1=I_2$. Proceeding inwards from the edges of the action plane, the first two states in the sequence bear a close resemblance to the first two states in Figure 8 at $I_2=0$ and $I_2=3$, respectively. The next state in the sequence is however of symmetric ''normal mode'' character, and is localized in the vicinity of the resonance intersection $\mathbf{I}^r$. There is therefore an effective 1:1 mixing along the direction $\mathcal{N}_{12}=\text{const}$ arising from the two 2:1 stretch-bend coupling terms. In fact, analysis of the interaction of the two 2:1 resonant coupling terms using classical perturbation theory gives an estimate of the effective strength of the induced 1:1 coupling.[56]

One can assign these states using labels which are essentially the same as in the integrable 2:1 case, but augmented with a $\pm$ subscript and ‡ superscript. The $\pm$ label describes the state symmetry with respect to exchange $1\leftrightarrow 2$ while the ‡ symbol denotes a state with ''normal mode'' character. The three states in Figure 12 can therefore be labelled $\langle 32,32,0\rangle_+$, $\langle 32,26,0\rangle_+$ and $\langle 32,20,0\rangle_+^{\ddagger}$, respectively.

In Figure 13 we show the corresponding Husimi distributions. Note that the Husimis, including the terminal state shown in Figure 13c, all show the common feature of localized density at $\phi_1=6\pi$. The terminal state phase space distribution also has some similarity to the corresponding integrable limit normal mode state Husimi shown in Figure 11d, albeit somewhat distorted and phase shifted in ϕ_1, and could be assigned the normal mode quantum numbers $[4,14,2]_+$. The terminal state is thus a mixed state for which *more than*

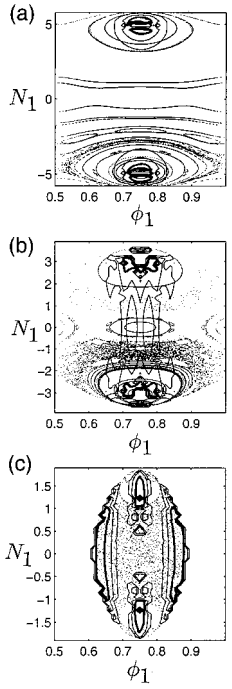

FIG. 13. Husimi distributions corresponding to the $\nu=0$ 2:1 resonance sequence shown in Figure 12.

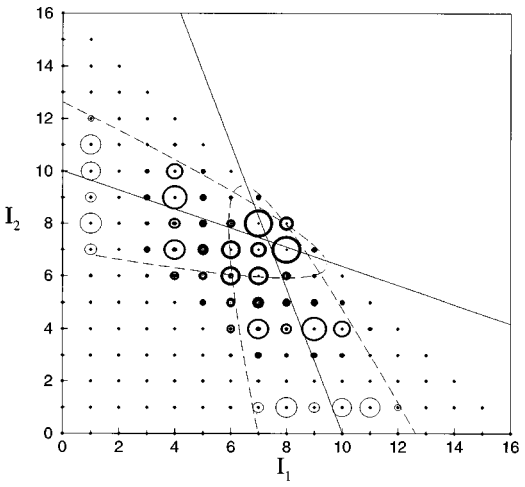

FIG. 14. Sequence of action space projections for eigenstates of the two 2:1 resonance channel Hamiltonian with $\nu=1$.

one set of quantum number labels is possible. We observe that the resonance excitation quantum number ν is different in each set of quantum numbers, i.e., $\nu=0$ (2:1 label) versus $\nu=2$ (1:1 label).

Figure 14 shows a sequence of 2 states $\langle 32,30,1\rangle_+$, $\langle 32,24,1\rangle_+$ that leads to a mixed normal mode-type state $\langle 32,18,1\rangle_+^{\ddagger}$ in the vicinity of $\mathbf{I}^r$. The associated Husimis are shown in Figure 15. The parent state (at $n_2=1$) Husimi shown in Figure 15a corresponds to $\nu=1$ as is clearly seen by comparing to the integrable case in Figure 7b. The parent state is relatively far away from the resonance junction and hence the close resemblance of the corresponding Husimi distributions. The Husimi for the next state in the sequence, Figure 15b, is localized in angle space but delocalized in action. We provisionally associate this delocalization in action space with the destruction of barriers to classical phase space transport.

The terminal state, which resembles a ''normal mode'' state in action space, localizes entirely on the upper sheet of the sos (Figure 15c). The Husimi function, however, is significantly distorted as compared to the corresponding integrable normal mode Husimi. Most noticeable is a shift in phase angle ϕ_1 from the integrable 1:1 case.

For the Hamiltonian with two 2:1 resonant stretch-bend coupling terms, we are therefore able to identify sequences of resonant states that define the ''parentage'' of particular mixed states. The terminal states are mixed, as suggested by their Husimi distribution functions, and can be viewed as part of one or more sequences. This leads to a *nonunique labelling* of the mixed states. For example, the terminal state of the sequence shown in Figure 12 can be assigned either as $\langle 32,20,0\rangle_+$ or as $[4,14,2]_+$. The basis for our identification of sequences is a study of amplitude distribution in action space, guided by the classical resonance channel template obtained via Chirikov analysis. It is not clear how an analysis based upon primary periodic orbit bifurcations alone[20] would enable such patterns to be identified.

We emphasize that the nonunique labelling of states obtained here and in the next section is a consequence of the intersection of the primary 1:1 and 2:1 resonance channels. This level of dynamical complexity is not present in the relatively straightforward $\mathsf{P}=8$ case treated previously by us[47] and others.[24,48] Our analysis and assignments therefore go beyond this earlier work.

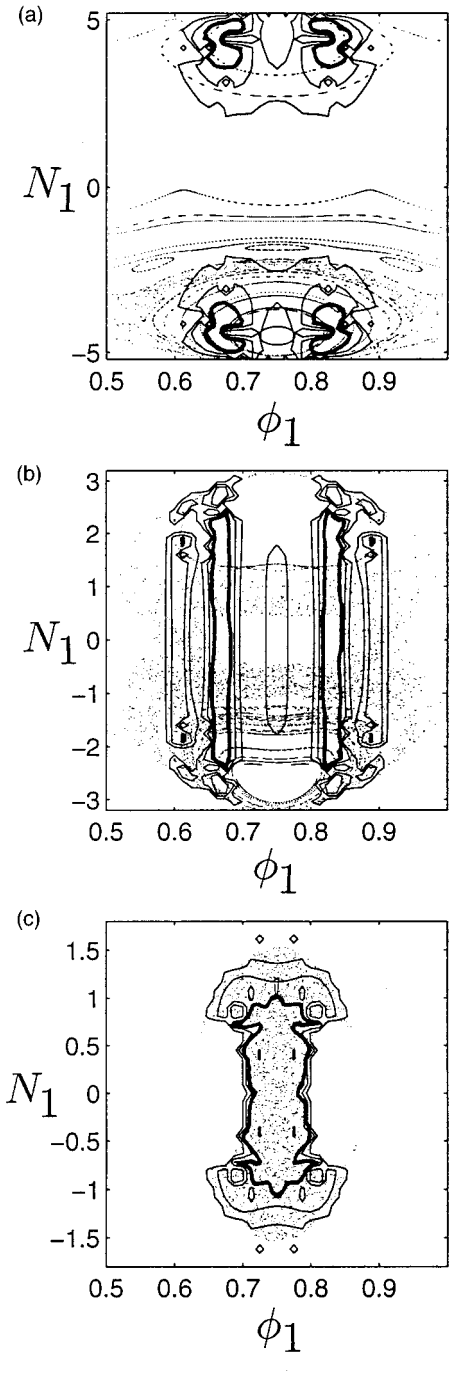

FIG. 15. Husimi distributions corresponding to the $\nu=1$ 2:1 resonance sequence shown in Figure 14.

VI. FULL BAGGOT HAMILTONIAN

The Chirikov resonance analysis of the Baggot Hamiltonian given in section III B suggests the existence of four

classes of eigenstate (cf. Ref. 37): (1) Nonresonant states, unaffected by any primary resonance. Phase space densities for such states are located outside any of the resonance channels, and good quantum numbers are the zeroth-order quantum numbers n_1, n_2 and n_b. States are labelled as (n_1,n_2,n_b). (2) Normal mode (1:1) resonant states, with phase space densities located in the 1:1 resonance channel. Approximate good quantum numbers are $\mathcal{N}$, $\mathcal{N}_{12}=n_1+n_2$ and a third quantum number ν describing the level of excitation inside the 1:1 resonance. The relevant states are labelled as $[\mathcal{N},\mathcal{N}_{12},\nu]$ or $[n_b,\mathcal{N}_{12},\nu]$. (3) Local-stretch/bend resonant states, with phase space densities located in the 2:1 resonance channel. Approximate good quantum numbers are $\mathcal{N},\mathcal{N}_{\sigma b}=2n_\sigma+n_b$, and a resonant excitation quantum number ν. States are therefore labelled by $\langle\mathcal{N},\mathcal{N}_{\sigma b},\nu\rangle$. (4) ''Mixed'' eigenstates, located in the vicinity of the resonance channel intersection. A similar classification has been proposed by Lu and Kellman[24] and by Rose and Kellman,[48] in either case without reference to the actual location of the resonance channels in action space.

Our classification scheme provides a framework within which to analyze the eigenstates of the Baggot Hamiltonian. In regions of phase space in which there is strong coupling between modes, the zeroth-order invariant structures that provide the basis of the classification scheme may be destroyed. Nevertheless, examination of quantum phase space densities often enables us to provide an unambiguous dynamical assignment. Such an approach has previously been successful for the $\mathsf{P}=8$ manifold,[47] and we examine here the set of states with $\mathsf{P}=16$.

A. Progressions of states along resonance channels

In the case of the integrable single resonance cases discussed in the previous section, the zeroth-order and/or resonance quantum numbers provide a rigorous and complete set of state labels. For the full Baggot Hamiltonian, which contains three linearly dependent resonance coupling terms and which is classically nonintegrable, states far away from the resonance intersection region of action space can be assigned using labels appropriate to the first 3 classes discussed above. As one approaches the overlap region the approximate labels may break down and we have a possibility of states belonging to class 4.

Nevertheless, as noted in the previous section, it is possible to identify sequences of states that progress along resonance channels, so that specific states in the resonance intersection region can be identified as the terminus of one (or more) sequence(s) of regular (assignable) states. It is important to note that it is quite possible for two different sequences to have a common terminal state; the two sets of associated labels then approximately describe the same eigenstate. Such ambiguity in the labelling of eigenfunctions distinguishes the $\mathsf{P}=16$ case currently under study from the dynamically simpler $\mathsf{P}=8$ manifold analyzed previously.[24,47,48]

We now proceed to combine insights gained from study of surfaces of section, Husimi phase space densities and the classical resonance template to analyze eigenstates of the full

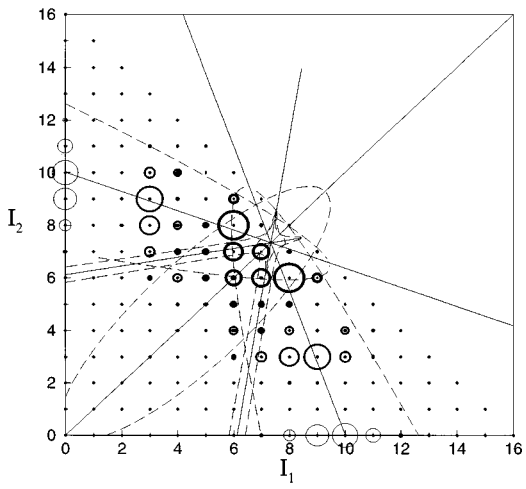

FIG. 16. Sequence of action space projections for the full Baggot Hamiltonian with $\nu=0$.

Baggot Hamiltonian with $\mathsf{P}=16$. We focus our attention on the fate of the three sequences presented in the last subsection as we turn on the remaining primary 1:1 resonance.

Figures 16 and 17 show the sequence of states progressing along the 2:1 resonance channels and their respective Husimi distributions. This sequence is to be compared to the similar one shown in the previous section (cf. Figures 12, 13). The first and second states are quite similar to their partners in the previous sequence. The terminal state is again a mixed state with nonunique labels; there are nevertheless clear differences in the forms of the Husimi due to the different phases of the induced 1:1 and primary 1:1 resonant coupling terms. In the full Hamiltonian the terminal Husimi is almost completely localized on the upper sos whereas in the $2\times2{:}1$ resonance case the terminal state is delocalized on both sheets of the sos.

In Figures 18 and 19 we show the $\nu=1$ sequence and the corresponding Husimis analogous to the sequence shown in Figure 14. For the full Hamiltonian, the form of the Husimi of the second state is indicative of an avoided crossing with another state. Computation of an energy level correlation diagram as a function of β_{sb} confirms this surmise. The resonant + parity state is involved in an avoided crossing with a nearby normal mode state. The terminal state is somewhat more localized in phase space than the counterpart shown in the previous section. The terminal state for the full Hamiltonian also looks ''cleaner'' in action space as compared to the $2\times2{:}1$ case.

The sequences considered here show how groups of quantum states can organize around the classical resonance template in action space. In the case of the Baggot Hamiltonian, explicit computations of the Husimi distribution functions further illuminate the phase space significance of such sequences. The local-bend resonant sequences are generalizations of the more familiar sequence of normal mode states. We have studied sequences in addition to those presented in this paper. For example, it is possible to find sequences which show an initially resonant state going out of

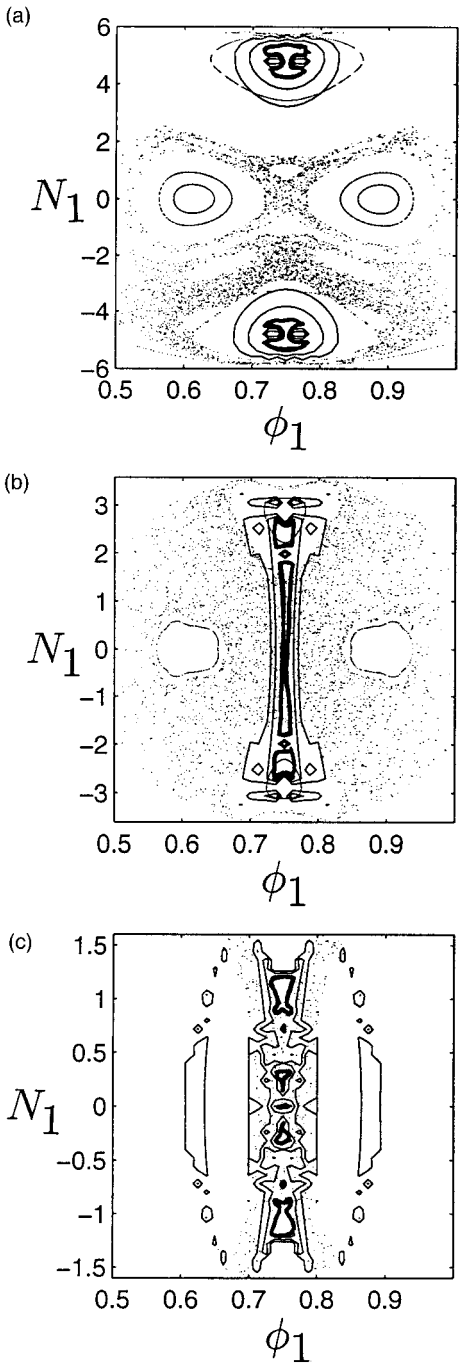

FIG. 17. Husimi distributions corresponding to the sequence shown in Figure 16.

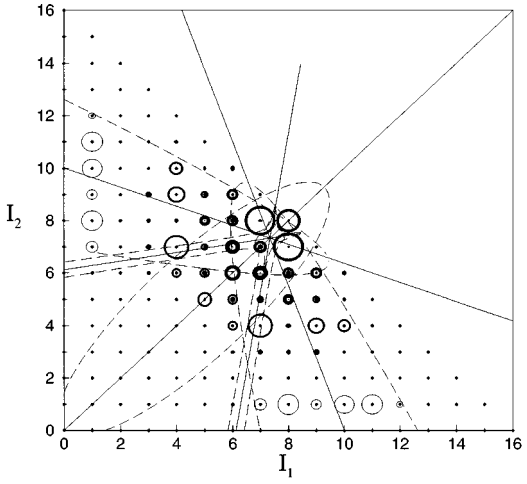

FIG. 18. Sequence of action space projections for the full Baggot Hamiltonian with $\nu=1$.

resonance and becoming a local nonresonant state (cf. Ref. 62). Aided by the Husimi distributions, one can usefully identify the parentage of very highly mixed states. Insight can be thereby obtained into the nature of mixed states in the vicinity of the resonance intersection by their identification as terminal states of a sequence(s) of regular states.

It is also apparent from the above examples that the approximate periodicity of the form of resonant eigenstates associated with the value of the slope of the resonance line is an important aid in identification of sequences of related states. The width of a particular resonance in action space determines the number of quantum states that can fit within the the resonance channel. In the Baggot case we have based our classical resonance analysis on the primary resonances (2:1 and 1:1), which have significant widths (compared to $\hbar$). High-order resonances will have narrow widths, in which case quantum states strongly influenced by the resonance lie outside the classical resonance zone.[45] However, such interacting quantum states will nevertheless organize themselves in accordance with the approximate periodicity of the resonance line, just as for the sequences of states inside the primary resonance channels. The corresponding Husimi functions will exhibit distorted but topologically non-resonant features. The periodicities in the form of the ''quantum resonant'' states analyzed by Roberts and Jaffé are clearly observable in Figure 6 of Ref. 45.

B. Energy level correlation diagrams and avoided crossings

We have studied energy level correlation diagrams for the Baggot Hamiltonian under variation of the parameter β_{sb}, which controls the strength of the 2:1 resonances. It is found that almost all of the narrowly avoided crossings that occur close to or at the physical value of β_{sb}, corresponding to the full Baggot Hamiltonian studied in the rest of the paper, involve three states. Two of the states have the same $[\pm]$ symmetry and are involved in either a broad or sharp crossing, while the third state, of opposite symmetry, is a partner state to one of the two states. Interaction between the two states of the same symmetry results in delocalization of the Husimi distribution for one of the partner states. Typically, at high energies and values of $\mathcal{N}$ such that $\mathbf{I}^r$ lies in the physical region of action space, the two states involved in the crossing are localized on one of the two sheets of the surface of section, with the other state delocalized over both sheets. An example would be a state with a very small number of bend quanta that interacts with a state with a large number of bend quanta. Another possibility is that all three

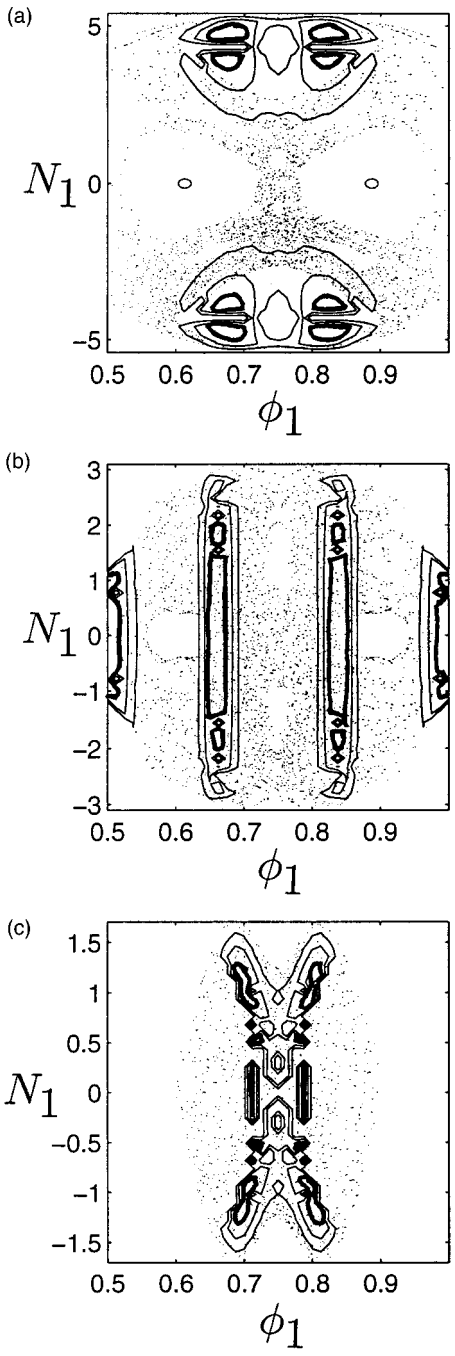

FIG. 19. Husimi distributions corresponding to the sequence shown in Figure 18.

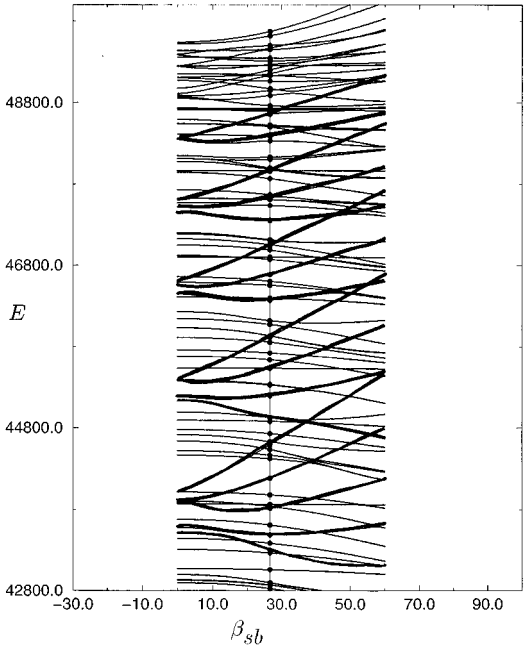

FIG. 20. Evolution of the energy spectrum as a function of the Baggot parameter β_{sb}. ''Diabats'' are shown as thick lines.

states can localize/delocalize on one sheet of the surface of section. An example for the latter case has been presented earlier (cf. Figure 4 in Ref. 47).

A considerable amount of work has been devoted in the recent literature to determining the quantal signatures of a classical nonlinear resonance.[63] Most of the studies have concentrated on the evolution of the eigenenergies of a quantum system under the variation of a parameter of the Hamiltonian. Attempts to correlate the type and number of avoided crossings to classical resonances have been unsatisfactory. In fact, as pointed out by Berry,[68] the fragility of one parameter crossings is partially responsible for the inconclusive results. The results of Ramachandran and Kay[64] and Ozorio de Almeida[69] make it clear that there is no necessary connection between the existence of avoided crossings of quantum energy levels and classical resonant dynamics.

It is nevertheless interesting to ask which features of the energy level correlation diagram might be associated with classical resonances. The results in this paper and in Ref. 64 suggest such a feature in the case when the classical resonances have significant widths in action space. Ramachandran and Kay noted that, under variation of a parameter corresponding to the frequency of one of 2 oscillators involved in a resonance, states deep inside the resonance zone exhibit nearly parallel curves in the correlation diagram. Figure 20 shows the energy correlation obtained by varying the parameter, β_{sb}, that controls the width of the 2:1 resonance zone. Variations of the states in the classical resonance zone are shown as thick lines (diabats). Note that these states undergo the largest amount of variation upon changing the resonance width parameter; groups of such states form a set of ''fans.'' The states within each group correspond to different levels of excitation inside the resonance zone, as discussed previously. The number of states in each group decreases with increasing energy, correlating with the decrease in the classical resonance width. It is significant to observe that a state from any given group of resonant states has many avoided crossings with local modes and normal modes. These avoided crossings are not in general associated with classical resonant motion as also pointed out by several authors.[70]

It is also relevant to point out that the sequences of states that progress along the 2:1 resonance channel consist pre-

cisely of those states corresponding to nearly parallel lines from different groups in Figure 20.

Finally, we note that the existence of many broad avoided crossings in the eigenvalue correlation diagrams we have computed for $P=16$ means that it is often impossible to follow diabats in order to correlate eigenstates of the full Hamiltonian with those of zeroth-order single resonance Hamiltonians, as done by Rose and Kellman for $P=8$.[48]

VII. CONCLUSIONS

In this paper we have studied the classical and quantum mechanics of the Baggot vibrational Hamiltonian for H_2O.[25] We have shown first of all that standard Chirikov resonance analysis provides a useful approximate map of the classical phase space structure. This conclusion is supported by more rigorous analysis of classical phase space structure in terms of families of resonant 2-tori, and by examination of classical surfaces of section. We point out that determination of the location of primary periodic orbits alone is not sufficient to establish detailed correlations between the form of the quantum eigenstates of the Baggot Hamiltonian and classical phase space structure. Whereas the primary periodic orbits intersect constant $\mathcal{N}$ (superpolyad number) surfaces in isolated points, resonant 2-tori determined within the single resonance approximation appear in 1-parameter families. The resonant 2-tori are thus suitable generalizations of the primary periodic orbits to 3D systems, and form a useful framework for understanding both the classical phase space and quantum-classical correspondence of the system.

An essential aspect of our study is the examination of quantum phase space (Husimi) distribution functions for eigenstates of the Baggot Hamiltonian. Comparison of quantum phase space distributions with corresponding classical surfaces of section enables us to define resonant and nonresonant states as localized inside or outside a given resonance channel, respectively. Quantum states are found to organize into sequences of states that progress along the resonance channels. An important observation is that the action space amplitudes for states in such sequences exhibit a periodicity, which is determined by the slope of the classical resonance line. The existence of these sequences enables us to provide labels for terminal ''mixed'' states in the vicinity of resonance intersections.

For the manifold of states examined (all states with $P=16$), it is found that most states can be assigned to one of 4 distinct classes of eigenstate; these assignments are made with the aid of the Husimi function and the identification of the various sequences. The study of the energy spectrum with the variation of a resonant coupling parameter (which determines the width of a resonance channel) provides a characteristic quantum signature of states deep in the resonance regions. A similar signature had been studied earlier by Ramachandran and Kay in a simpler system.[64] Our studies strengthen the notion that there is no necessary connection between the existence of avoided crossings in energy level correlation diagrams and particular classical non-linear resonances. However, the approximate periodicity associated with the slope of the classical resonance line in action space does influence the quantum states irrespective of the widths of the resonances, and is an important parameter in the studies of quantum-classical correspondence of resonant Hamiltonians.

The existence of the superpolyad quantum number $\mathcal{N}$ reduces the 3-mode Baggot Hamiltonian to an effectively two degree of freedom problem, and we have made extensive use throughout of the technology developed for studying the classical mechanics and classical-quantum correspondence of such systems. Despite being effectively a two degree of freedom problem, however, the phase space structure exhibits complexities not usually found in 2-mode systems.[13] Future work will investigate the consequences of breaking the constancy of $\mathcal{N}$, thereby obtaining a true 3-mode problem. Very little is currently known concerning detailed classical dynamics and/or quantum-classical correspondence for 3-mode molecular Hamiltonians. Most techniques that are useful for 2 degree of freedom systems are either inappropriate or need to be suitably generalized in order to study multimode problems. A number of very rich problems pertaining to the nature of classical phase space transport, dynamical tunneling, chaos assisted tunneling[71] and multimode effects arise, however, and the undoubtedly subtle interplay between classical transport and quantum mechanisms leading to delocalization and/or localization has to be understood in order to gain insights into the spectrum and dynamics of realistic molecular Hamiltonians. The present work provides the foundation for future work towards these important yet difficult goals.

ACKNOWLEDGMENTS

This work is supported by NSF Grant CHE-9403572. Computations reported here were performed in part on the Cornell Supercomputer Facility, which is supported by NSF and IBM corporation.

APPENDIX: PRIMARY PERIODIC ORBITS AND RESONANT 2-TORI

1. Bifurcation analysis of the Baggot Hamiltonian: Periodic orbits

In terms of variables $(\mathbf{N},\boldsymbol{\phi})$, with $\mathbf{N}=\mathbf{K}+\mathbf{J}^r$, the Baggot Hamiltonian is

$$\begin{aligned}\mathcal{H}=&2\tilde{\omega}N_2+\alpha_1N_1^2+\alpha_2N_2^2+\beta_{12}(N_2)\\&\times[(N_2+BJ)^2-N_1^2]^{1/2}\cos\phi_1+\beta_{22}[(N_2+BJ)^2-N_1^2]\\&\times\cos 2\phi_1+\beta_b(AJ-4N_2)[(N_2+N_1+BJ)^{1/2}\\&\times\cos\phi_++(N_2-N_1+BJ)^{1/2}\cos\phi_-],\end{aligned}\tag{A1}$$

with $\beta_{12}(N_2)\equiv\beta'_{12}+\mu_1N_2+\mu_2$, $\phi_\pm\equiv(\phi_1\pm\phi_2)/2$, and $\beta_{1b}=\beta_{2b}\equiv\beta_b$. The various constants are functions of the original Baggot parameters:

$$\tilde{\omega}=\Omega_s-2\Omega_b,\tag{A2a}$$

$$\alpha_{1,2}=2\tilde{c}\mp\tilde{c}_{12},\tag{A2b}$$

$$\mu_1 = 2(\lambda' - 2\lambda''), \tag{A2c}$$

$$\mu_2 = (2\lambda' B + \lambda'' A)J. \tag{A2d}$$

In terms of the original action variables, $(AJ-4N_2)=I_b$ and $(N_2 \pm N_1 + BJ) = I_{1,2}$.

Hamilton's equations of motion are:

$$\begin{aligned}\dot{\phi}_1 = {} & 2\alpha_1 N_1 - N_1 \beta_{12}[(N_2+BJ)^2 - N_1^2]^{-1/2} \\ & \times \cos(\phi_1) - 2N_1\beta_{22}\cos(2\phi_1) + \frac{1}{2}\beta_b(AJ-4N_2) \\ & \times [(N_2+N_1+BJ)^{-1/2}\cos(\phi_+) \\ & -(N_2-N_1+BJ)^{-1/2}\cos(\phi_-)],\end{aligned} \tag{A3a}$$

$$\begin{aligned}\dot{\phi}_2 = {} & 2\tilde{\omega} + 2\alpha_2 N_2 + 2\beta_{22}(N_2+BJ)\cos(2\phi_1) + [\mu_1[(N_2 \\ & + BJ)^2 - N_1^2]^{1/2} + \beta_{12}(N_2+BJ)[(N_2+BJ)^2 - N_1^2]^{-1/2}] \\ & \times \cos(\phi_1) - 4\beta_b[(N_2+N_1+BJ)^{1/2}\cos(\phi_+) + (N_2 \\ & - N_1 + BJ)^{1/2}\cos(\phi_-)] + \frac{1}{2}\beta_b(AJ-4N_2)[(N_2+N_1 \\ & + BJ)^{-1/2}\cos(\phi_+) + (N_2-N_1+BJ)^{-1/2}\cos(\phi_-)],\end{aligned} \tag{A3b}$$

$$\begin{aligned}\dot{N}_1 = {} & \beta_{12}[(N_2+BJ)^2 - N_1^2]^{1/2}\sin(\phi_1) \\ & + 2\beta_{22}[(N_2+BJ)^2 - N_1^2]\sin(2\phi_1) \\ & + \frac{1}{2}\beta_b(AJ-4N_2)[(N_2+N_1+BJ)^{1/2}\sin(\phi_+) \\ & + (N_2-N_1+BJ)^{1/2}\sin(\phi_-)],\end{aligned} \tag{A3c}$$

$$\begin{aligned}\dot{N}_2 = {} & \frac{1}{2}\beta_b(AJ-4N_2)[(N_2+N_1+BJ)^{1/2}\sin(\phi_+) \\ & - (N_2-N_1+BJ)^{1/2}\sin(\phi_-)].\end{aligned} \tag{A3d}$$

a. Normal mode periodic orbits

We are interested in finding the equilibrium points of the above set of equations ($\dot{N}_k = 0 = \dot{\phi}_k$, $k=1,2$) since they correspond to periodic orbits of the full system, i.e., 1-tori with the angle variable being the ignorable angle $\psi \equiv A\theta_b + B(\theta_1+\theta_2)$ conjugate to the polyad number J. We first look for solutions corresponding to $N_1 = 0$, which are normal mode type solutions in the full system. If we set $N_1 = 0$ in the above equations then we get the system of equations:

$$\dot{\phi}_1 = -\beta_b(AJ-4N_2)(N_2+BJ)^{-1/2}\sin(\phi_1/2)\sin(\phi_2/2), \tag{A4a}$$

$$\begin{aligned}\dot{\phi}_2 = {} & 2\tilde{\omega} + 2\alpha_2 N_2 + [\mu_1(N_2+BJ) + \beta_{12}]\cos(\phi_1) \\ & + 2\beta_{22}(N_2+BJ)^2\cos(2\phi_1) - [8\beta_b(N_2+BJ)^{1/2} \\ & + \beta_b(AJ-4N_2)(N_2+BJ)^{-1/2}]\cos(\phi_1/2)\cos(\phi_2/2),\end{aligned} \tag{A4b}$$

$$\begin{aligned}\dot{N}_1 = {} & \beta_{12}(N_2+BJ)\sin(\phi_1) + 2\beta_{22}(N_2+BJ)^2\sin(2\phi_1) \\ & + \beta_b(AJ-4N_2)(N_2+BJ)^{1/2}\sin(\phi_1/2)\cos(\phi_2/2),\end{aligned} \tag{A4c}$$

$$\dot{N}_2 = \beta_b(AJ-4N_2)(N_2+BJ)^{1/2}\cos(\phi_1/2)\sin(\phi_2/2), \tag{A4d}$$

where we have used the standard trigonometric identities to rewrite terms involving $\phi_\pm$. Note that β_{12} is a function of N_2. Let us consider the equation for $\dot{N}_2$ and note that it vanishes for the following cases:

(a) $N_2 = AJ/4$,
(b) $N_2 \neq AJ/4$, $\phi_1 = \pm\pi$,
(c) $N_2 \neq AJ/4$, $\phi_2 = 0, \pm 2\pi$.

We have not considered the possibility of $N_2 + BJ = 0$ since this corresponds to $I_b = J$, $I_1 = I_2 = 0$, i.e., a pure bend critical point.

Case a: In this case $N_2 = AJ/4$ which implies that the action in the bend mode is zero. With $\phi_1 = 0, \pm\pi$ we see that $\dot{N}_k = 0 = \dot{\phi}_1$ $(k=1,2)$ and

$$\begin{aligned}\dot{\phi}_2 = {} & 2\tilde{\omega} + \frac{1}{2}(\alpha_2 A + \beta_{22})J + \frac{1}{4}\mu_1 J + \beta_{12} \\ & - 4\beta_b J^{1/2}\cos(\phi_2/2).\end{aligned} \tag{A5}$$

Although the time derivative $\dot{\phi}_2$ is in general nonzero, the solution with $I_b = 0$ is nevertheless a periodic orbit, and $\dot{\phi}_2$ is just the rotation rate around the periodic orbit. There are, however, certain values of $\phi_2 \equiv \phi_2^{(1)}$ such that $\dot{\phi}_2 = 0$, signalling the bifurcation of the normal mode periodic orbit due to 2:1 resonance with the bend mode. This value of ϕ_2 is determined by:

$$\cos(\phi_2^{(1)}) = \frac{1}{4\beta_b J^{1/2}}(C_0 + C_1 J), \tag{A6}$$

where

$$C_0 = 2\tilde{\omega} + \beta_{12}' + \mu_2, \tag{A7a}$$

$$C_1 = \frac{1}{2}(\alpha_2 A + \beta_{22}) + \frac{1}{4}\mu_1(1+A). \tag{A7b}$$

If both $\dot{\phi}_1 = 0 = \dot{\phi}_2$ when $I_b = 0$ then $\phi_1 = \theta_1 - \theta_2$ and $\phi_2 = \theta_1 + \theta_2 - 4\theta_b$. Thus, vanishing of both time derivatives implies that $\dot{\theta}_1 = \dot{\theta}_2 = 2\dot{\theta}_b$.

Case b: It is easy to convince oneself that in case b) both $\dot{N}_1$ and $\dot{\phi}_1$ cannot vanish with a single choice of ϕ_2 and hence we disregard this case.

Case c: In this case with a choice of $\phi_1 = 0, \pm 2\pi$ we have $\dot{N}_k = 0 = \dot{\phi}_1$, $k=1,2$, and the equation we are left with is as follows:

$$\begin{aligned}\dot{\phi}_2 = {} & 2\tilde{\omega} + 2\alpha_2 N_2 + \mu_1(N_2+BJ) + \beta_{12} + 2\beta_{22}(N_2+BJ) \\ & \mp 8\beta_b(N_2+BJ)^{1/2} \pm \beta_b(AJ-4N_2)(N_2+BJ)^{-1/2}.\end{aligned} \tag{A8}$$

We cannot have $N_2 = AJ/4$ here since this was considered in the previous case and moreover, this solution for N_2 gives us

precisely the periodic orbits corresponding to the bifurcation of the normal mode periodic orbit family resulting from case a) due to the 2:1 resonances. Simplifying the above equation and denoting $x \equiv (N_2 + BJ)$ we get a cubic equation in $x^{1/2}$:

$$x^{3/2} \mp p x + q x^{1/2} \pm r = 0, \tag{A9}$$

where

$$p = \frac{12\beta_b}{2(\alpha_2 + \mu_1 + \beta_{22})}, \tag{A10a}$$

$$q = \frac{C_0 - (\mu_1 + 2\alpha_2)BJ}{2(\alpha_2 + \mu_1 + \beta_{22})}, \tag{A10b}$$

$$r = \frac{\beta_b J}{2(\alpha_2 + \mu_1 + \beta_{22})}, \tag{A10c}$$

with the condition that $x \neq 0$.

b. Local mode periodic orbits

Referring back to the full system of Hamilton's equations of motion we observe that with $N_2 = AJ/4$ and $\phi_1 = 0, \pm\pi$ we have $\dot{N}_k = 0$, and the equation for $\dot{\phi}_1$ becomes:

$$\dot{\phi}_1 = N_1 \left[2(\alpha_1 - \beta_{22}) \mp \beta_{12} \left(\frac{J^2}{16} - N_1^2 \right)^{-1/2} \right]. \tag{A11}$$

For $N_1 = \pm \overline{N_1}$ with

$$\overline{N_1} = \left[\frac{J^2}{16} - \frac{\beta_{12}^2}{4(\alpha_1 - \beta_{22})^2} \right]^{1/2}, \tag{A12}$$

we have $\dot{\phi}_1 = 0$ and so obtain local mode periodic orbit solutions. Note, again that the finite value of $\dot{\phi}_2$ here does not matter as $I_b = 0$. As before there are certain values of $\phi_2 \equiv \phi_2^{(2)}$ such that $\dot{\phi}_2 = 0$ and this indicates that the local mode periodic orbits can bifurcate due to the influence of the 2:1 resonances. In the case when $\phi_1 = 0$ we have:

$$\cos(\phi_2^{(2)}/2) = \frac{f_1(J)}{f_2(J)}, \tag{A13}$$

where

$$f_1(J) = 2\tilde{\omega} + \frac{1}{2}(\alpha_2 A + \alpha_1)J + \frac{\mu_1 \beta_{12}}{2(\alpha_1 - \beta_{22})}, \tag{A14a}$$

$$f_2(J) = 4\beta_b \left[\left(\frac{J}{4} + \overline{N_1} \right)^{1/2} + \left(\frac{J}{4} - \overline{N_1} \right)^{1/2} \right], \tag{A14b}$$

with a similar equation for the case when $\phi_1 = \pm\pi$. In order to calculate the periodic orbits resulting from the bifurcation of the local mode solutions due to the 2:1 resonances we have to consider the full system of equations and solve them with the condition $N_2 \neq AJ/4$. Let us consider the equations for $\dot{N}_k$ $(k = 1,2)$ and remember that the allowed ranges for the conjugate angles are $\phi_1 \in (-2\pi, 2\pi)$ and $\phi_2 \in (-8\pi, 4\pi)$. Of all the possible combinations, it is sufficient to consider two cases with a) $\phi_1 = 0 = \phi_2$ and b) $\phi_1 = 0$, $\phi_2 = 2\pi$. These choices for the angles imply that $\dot{N}_k = 0$; $k = 1,2$ and the relevant equations for the time derivative of the angles reduces to a pair of nonlinear equations in the variables $t = x_+ + x_-$, $s = x_+^2 + x_-^2$ with $x_\pm \equiv (N_2 \pm N_1 + BJ)^{1/2}$. The two cases are related by changes in the sign of β_b and the nonlinear equations to be solved are:

$$d_1 t^3 + d_2 ts + d_3 t \pm 2\beta_b s \pm \beta_b J = 0, \tag{A15a}$$

$$e_1 t^4 \mp 2\beta_b t^3 + e_2 s t^2 - e_2 s^2 + e_3 t^2 \pm \beta_b ts + e_4 s \pm \frac{1}{2}\beta_b J t = 0, \tag{A15b}$$

where

$$d_1 = \alpha_1 - \beta_{22}, \tag{A16a}$$

$$d_2 = -\left[d_1 + \frac{1}{2}\mu_1 \right], \tag{A16b}$$

$$d_3 = \mu_1 BJ - \beta'_{12} - \mu_2, \tag{A16c}$$

$$e_1 = \frac{1}{4}\mu_1, \tag{A16d}$$

$$e_2 = \frac{1}{2}(\alpha_2 + \beta_{22} - \mu_1), \tag{A16e}$$

$$e_3 = \tilde{\omega} - \alpha_2 BJ, \tag{A16f}$$

$$e_4 = -\frac{1}{2} d_3 - e_3. \tag{A16g}$$

The pair of nonlinear equations are solved numerically with the conditions $x_\pm \neq 0$.

2. Integrable limit 2-tori

Consider the Baggot Hamiltonian with only the 1:1 and the 2:2 resonance interactions included, i.e., $\beta_b = 0$. Using the generating function:

$$\mathscr{T}_r = (\theta_1 - \theta_2)L_1 + (\theta_1 + \theta_2)L_2 + \theta_b L_b, \tag{A17}$$

the Hamiltonian becomes:

$$\begin{aligned} \mathscr{H}_{\text{int}} = {} & 2\Omega_s L_2 + \Omega_b L_b + (2\alpha_s - \epsilon_{ss})L_1^2 + (2\alpha_s + \epsilon_{ss})L_2^2 \\ & + \alpha_b L_b^2 + 2\epsilon_{sb} L_b L_2 + \beta_{12}(L_2^2 - L_1^2)^{1/2} \cos(\chi_1) \\ & + \beta_{22}(L_2^2 - L_1^2)\cos(2\chi_1). \end{aligned} \tag{A18}$$

It is clear that both L_2 and L_b are constants of the motion, and the superpolyad number $J = 4L_2 + L_b$. Thus, finding the equilibrium points of the above Hamiltonian determines resonant 2-tori since there are *two* ignorable angles. It is easy to solve the pair of equations $\dot{L}_1 = 0 = \dot{\chi}_1$ and the solutions are with $\chi_1 = 0, \pm\pi$:

$$\text{a)} \quad L_1 = 0, \tag{A19a}$$

$$\text{b)} \quad L_1 = \pm \left[L_2^2 - \frac{\beta_{12}^2}{4(2\alpha_s - \epsilon_{ss} - \beta_{22})^2} \right]^{1/2}. \tag{A19b}$$

The first solution corresponds to normal mode 2-tori and the second solution represents local mode 2-tori.

Now, consider the Baggot Hamiltonian with a single 2:1 resonance interaction only and perform a canonical transformation

$$\mathscr{G}_r=(\theta_1-2\theta_b)K_1+\theta_2K_2+(\theta_1+2\theta_b)K_b, \tag{A20}$$

which gives the transformed Hamiltonian:

$$\mathscr{H}_{\rm int}=\widetilde{C}K_1+\widetilde{B}K_1^2+h(K_2,K_b)+2\beta_b(K_b-K_1)\times(K_b+K_1)^{1/2}\cos(\zeta_1). \tag{A21}$$

Here, $\widetilde{B}\equiv\alpha_s-2\epsilon_{sb}+4\alpha_b$, $\widetilde{C}\equiv\widetilde{\Omega}+\widetilde{A}K_b+(\epsilon_{ss}-2\epsilon_{sb})K_2$, $\widetilde{\Omega}\equiv\Omega_s-2\Omega_b$, $\widetilde{A}\equiv2(\alpha_s-4\alpha_b)$, and $h(K_b,K_2)$ is a constant due to the fact that the new Hamiltonian is ignorable in the angles conjugate to K_b,K_2.

Again, solving the pair of equations $\dot{K}_1=0=\dot{\zeta}_1$ is relatively straightforward and one obtains:

$$\text{a)}\quad K_1=K_b,\ \cos(\zeta_1)=\frac{1}{2\beta_b(2K_b)^{1/2}}(\widetilde{C}+2\widetilde{B}K_b), \tag{A22a}$$

$$\text{b)}\quad 2\widetilde{B}y^{3/2}\mp3\beta_by+(\widetilde{C}-2\widetilde{B}K_b)y^{1/2}\pm2\beta_bK_b=0,\quad \chi_1=0,\pm\pi. \tag{A22b}$$

Solution a) corresponds to 2-tori with no bend quanta ($I_b=0$), while solutions b) are local-mode/bend resonant 2-tori. In this case one has $J=2K_2+4K_b$.

Thus, one gets 2-parameter families of resonant 2-tori, and we can plot the location of these solutions in action space as a function of one of the constants of motion and the polyad number. The results are summarized in Figure 2 where we show the families of periodic orbits and 2-tori in $(\mathscr{N},I_1,I_2)$ space.

From Figure 2 it is clear that the local mode periodic orbits ($I_1=0$ or $I_2=0$) of the full system lie at the boundaries of the families of 2-tori of the integrable subsystem. Moreover, the locus of periodic orbits resulting from the bifurcation of the normal mode solutions is given to reasonable approximation by the intersection of the sheets of resonant 2-tori. This confirms the appropriateness of the Chirikov analysis for the Baggot Hamiltonian.

[1] R. D. Levine and R. B. Bernstein, *Molecular Reaction Dynamics and Reactivity* (Oxford University Press, Oxford, 1987).
[2] D. Papousek and M. R. Aliev, *Molecular Vibrational-Rotational Spectra* (Elsevier, New York, 1982).
[3] C. E. Hamilton, J. L. Kinsey, and R. W. Field, Annu. Rev. Phys. Chem. **37**, 493 (1986).
[4] See, T. Uzer, Phys. Rep. **199**, 73 (1991); K. K. Lehmann, G. Scoles, and B. H. Pate, Annu. Rev. Phys. Chem. **45**, 241 (1994), and references therein.
[5] A. M. Ozorio de Almeida, *Hamiltonian Systems: Chaos and Quantization* (Cambridge University Press, Cambridge, 1988).
[6] M. J. Davis and E. J. Heller, J. Chem. Phys. **75**, 246 (1981); E. J. Heller, J. Phys. Chem. **99**, 2625 (1995).
[7] R. L. Sundberg, E. Abramson, J. L. Kinsey, and R. W. Field, J. Chem. Phys. **83**, 466 (1985); G. Sitja and J. P. Pique, Phys. Rev. Lett. **73**, 232 (1994).
[8] M. J. Davis, Chem. Phys. Lett. **192**, 479 (1992); Int. Rev. Phys. Chem. **14**, 15 (1995).
[9] M. C. Gutzwiller, *Chaos in Classical and Quantum Mechanics* (Springer, Berlin, 1990).
[10] See, J. M. Gomez Llorente and E. Pollak, Annu. Rev. Phys. Chem. **43**, 91 (1992), and references therein; S. C. Farantos, Int. Rev. Phys. Chem. **15**, 345 (1996).
[11] M. A. Sepulveda and F. Grossmann, Adv. Chem. Phys. **XCVI**, 191 (1996), and references therein.
[12] M. E. Kellman, in *Molecular Dynamics and Spectroscopy by Stimulated Emission Pumping*, edited by H.-L. Dai and R. W. Field (World Scientific, Singapore, 1995).
[13] B. Zhilinskii, Spectrochim. Acta. A **52**, 881 (1996); D. A. Sadovskii and B. Zhilinskii, Phys. Rev. A **48**, 1035 (1993); B. Zhilinskii, Chem. Phys. **137**, 1 (1989).
[14] D. E. Logan and P. G. Wolynes, J. Chem. Phys. **93**, 4994 (1990).
[15] S. A. Schofield and P. G. Wolynes, J. Chem. Phys. **98**, 1123 (1993).
[16] S. A. Schofield, P. G. Wolynes, and R. E. Wyatt, Phys. Rev. Lett. **74**, 3720 (1995); S. A. Schofield, R. E. Wyatt, and P. G. Wolynes, J. Chem. Phys. **105**, 940 (1996).
[17] D. M. Leitner and P. G. Wolynes, Phys. Rev. Lett. **76**, 216 (1996); Chem. Phys. Lett. **258**, 18 (1996).
[18] P. W. Anderson, Phys. Rev. **109**, 1492 (1958); P. A. Lee and T. V. Ramakrishnan, Rev. Mod. Phys. **57**, 287 (1985).
[19] C. Jaffé, J. Chem. Phys. **89**, 3395 (1988); M. E. Kellman and E. D. Lynch, J. Chem. Phys. **89**, 3396 (1988).
[20] L. Xiao and M. E. Kellman, J. Chem. Phys. **90**, 6086 (1989); Z. Li, L. Xiao, and M. E. Kellman, *ibid*. **92**, 2251 (1990); L. Xiao and M. E. Kellman, *ibid*. **93**, 5805 (1990); J. P. Rose and M. E. Kellman, *ibid*. **103**, 7255 (1995).
[21] M. Joyeux, Chem. Phys. **185**, 263 (1994); **167**, 299 (1992); **203**, 281 (1996); Chem. Phys. Lett. **247**, 454 (1995).
[22] B. R. Johnson and J. L. Kinsey, J. Chem. Phys. **91**, 7638 (1989); M. Baranger, M. R. Haggerty, B. Lauritzen, D. C. Meredith, and D. Provost, CHAOS **5**, 261 (1995).
[23] D. C. Rouben and G. S. Ezra, J. Chem. Phys. **103**, 1375 (1995); G. S. Ezra, *ibid*. **104**, 26 (1996).
[24] Zi-Min Lu and M. E. Kellman, Chem. Phys. Lett. **247**, 195 (1995).
[25] J. E. Baggot, Mol. Phys. **65**, 739 (1988).
[26] Zi-Min Lu and M. E. Kellman, J. Chem. Phys. (in press).
[27] B. V. Chirikov, Phys. Rep. **52**, 263 (1979).
[28] R. Mackay, J. D. Meiss, and I. C. Percival, Physica **13D**, 55 (1984).
[29] S. Wiggins, *Normally Hyperbolic Invariant Manifolds in Dynamical Systems* (Springer, Berlin, 1994), and references therein.
[30] R. E. Gillilan and G. S. Ezra, J. Chem. Phys. **94**, 2648 (1991).
[31] D. Begie, Chaos, Solitons and Fractals **5**, 177 (1995); J. Nonlinear Sci. **5**, 57 (1995).
[32] S. Wiggins, *Introduction to Applied Nonlinear Dynamical Systems and Chaos* (Springer, Berlin, 1990).
[33] V. I. Arnold, Russ. Math. Survey **18**, 85 (1963); N. N. Nekhoroshev, *ibid*. **32**, 1 (1977).
[34] A. J. Lichtenberg and M. A. Lieberman, *Regular and Stochastic Motion* (Springer, Berlin, 1983).
[35] V. I. Arnold, Dokl. Nauk. Akad. SSSR **156**, 9 (1964).
[36] P. Lochak, Phys. Lett. A **143**, 39 (1990); L. Chierchia and G. Gallavotti, Ann. Inst. Henri Poincaré Phys. Theor. **160**, 1 (1994); J. Laskar, Physica D **67**, 257 (1993); G. Haller, Phys. Lett. A **200**, 34 (1995).
[37] D. W. Oxtoby and S. A. Rice, J. Chem. Phys. **65**, 1676 (1976).
[38] C. Jaffé and P. Brumer, J. Chem. Phys. **73**, 5646 (1980).
[39] E. L. Sibert III, W. P. Reinhardt, and J. T. Hynes, J. Chem. Phys. **81**, 1115 (1984); E. L. Sibert III, J. T. Hynes, and W. P. Reinhardt, *ibid*. **81**, 1135 (1984).
[40] C. C. Martens, M. J. Davis, and G. S. Ezra, Chem. Phys. Lett. **142**, 519 (1987).
[41] Y. M. Engel and R. D. Levine, Chem. Phys. Lett. **164**, 270 (1989).
[42] C. C. Martens, J. Stat. Phys. **68**, 207 (1992).
[43] K. M. Atkins and D. E. Logan, Phys. Lett. A **162**, 255 (1992).
[44] D. E. Weeks and R. D. Levine, in *Structure and Dynamics of Non-Rigid Molecular Systems*, (Kluwer, Dordrecht, 1994), p. 249.
[45] F. L. Roberts and C. Jaffé, J. Chem. Phys. **99**, 2495 (1993).
[46] J. Laskar, Icarus **88**, 266 (1990); J. Laskar, C. Froeschlé, and A. Celletti, Physica D **56**, 253 (1992).
[47] S. Keshavamurthy and G. S. Ezra, Chem. Phys. Lett. **259**, 81 (1996).
[48] J. Rose and M. E. Kellman, J. Chem. Phys. **105**, 7348 (1996).
[49] D. J. Thouless, Phys. Rep. **13**, 93 (1974).
[50] K. Husimi, Proc. Phys. Math. Soc. Jpn. **22**, 264 (1940).
[51] L. E. Fried and G. S. Ezra, J. Chem. Phys. **86**, 6270 (1987); M. E. Kellman, *ibid*. **93**, 6630 (1990).
[52] B. T. Darling and D. M. Dennison, Phys. Rev. **57**, 128 (1940).
[53] A. Weinstein, Inv. Math. **20**, 47 (1973); J. Moser, Comm. Pure. Appl. Math. **29**, 727 (1976).
[54] C. C. Martens and G. S. Ezra, J. Chem. Phys. **86**, 279 (1986).

[55] S. P. Neshyba and N. De Leon, J. Chem. Phys. **86**, 6295 (1987).
[56] S. Keshavamurthy and G. S. Ezra (unpublished).
[57] M. Joyeux, J. Phys. A **29**, 5963 (1996).
[58] D. F. Escande, Phys. Rep. **121**, 165 (1985).
[59] E. P. Wigner, Phys. Rev. **40**, 749 (1932).
[60] K. Takahashi, J. Phys. Soc. Jpn. **55**, 762 (1986).
[61] A. Perelomov, *Generalized Coherent States and Their Applications* (Springer, Berlin, 1986).
[62] M. J. Davis, J. Phys. Chem. **92**, 3124 (1988).
[63] D. W. Noid, M. L. Koszykowski, M. Tabor, and R. A. Marcus, J. Chem. Phys. **72**, 6168 (1980); R. Ramaswamy and R. A. Marcus, *ibid*. **74**, 1379 (1981); B. Eckhardt, Phys. Rep. **163**, 205 (1988); T. Uzer, D. W. Noid, and R. A. Marcus, J. Chem. Phys. **79**, 4412 (1983); C. Jaffé and M. Watanabe, *ibid*. **86**, 4499 (1987).
[64] B. Ramachandran and K. G. Kay, J. Chem. Phys. **99**, 3659 (1993).
[65] It is possible to give a simple proof for the observed periodicity of the quantum states in the case of a single resonance, integrable case (unpublished notes). Analysis of the corresponding quantum Hamiltonian (Mathieu equation) along the lines of Ref. 64 demonstrates the effect of $\wp$ on the phase (γ in Ref. 64) of the wavefunction and the shift in the action I_z. For the example of the integrable 2:1 system it turns out that both the phase and the shift are 0 (mod $\wp$) when K_2 increments by $\wp$.
[66] J. Svitak, Z. Li, J. Rose, and M. E. Kellman, J. Chem. Phys. **102**, 4340 (1995).
[67] G. S. Ezra, J. Chem. Phys. **104**, 26 (1996).
[68] M. V. Berry, AIP Conf. Proc. **46**, 16 (1978).
[69] A. M. Ozorio de Almeida, J. Phys. Chem. **88**, 6139 (1984).
[70] R. T. Lawton and M. S. Child, Mol. Phys. **44**, 709 (1981); D. Farrelly and T. Uzer, J. Chem. Phys. **85**, 308 (1986); D. W. Noid, M. L. Koszykowski, and R. A. Marcus, *ibid*. **79**, 4412 (1983); M. J. Davis and E. J. Heller, *ibid*. **75**, 246 (1981); B. Ramachandran and K. G. Kay, Phys. Rev. A **41**, 1757 (1990); D. Farrelly and W. P. Reinhardt, J. Chem. Phys. **78**, 606 (1983); E. J. Heller, Faraday Discuss. Chem. Soc. **75**, 141 (1983); M. Wilkinson, J. Phys. A **20**, 635 (1987).
[71] S. Tomsovic and D. Ullmo, Phys. Rev. E **50**, 145 (1994); R. Utermann, T. Dittrich, and P. Hänggi, *ibid*. **49**, 273 (1994); M. Latka, P. Grigolini, and B. J. West, Phys. Rev. A **50**, 1071 (1994).